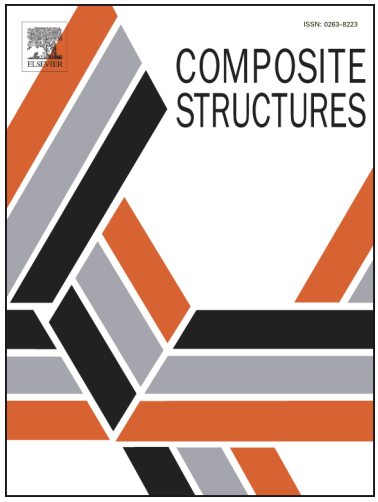


# Torsional Vibration of Size-dependent Viscoelastic Rods using Nonlocal Strain and Velocity Gradient Theory

S. El-Borgi, P. Rajendran, M.I. Friswell, M. Trabelssi, J.N. Reddy

PII: S0263-8223(17)33221-X
DOI: https://doi.org/10.1016/j.compstruct.2017.12.002
Reference: COST 9159

To appear in: *Composite Structures*

Please cite this article as: El-Borgi, S., Rajendran, P., Friswell, M.I., Trabelssi, M., Reddy, J.N., Torsional Vibration of Size-dependent Viscoelastic Rods using Nonlocal Strain and Velocity Gradient Theory, *Composite Structures* (2017), doi: https://doi.org/10.1016/j.compstruct.2017.12.002

# Torsional Vibration of Size-dependent Viscoelastic Rods using Nonlocal Strain and Velocity Gradient Theory

**S. El-Borgi**[a,1], **P. Rajendran**[a,b], **M.I. Friswell**[c], **M. Trabelssi**[d,e], **J.N. Reddy**[f]

[a] Mechanical Engineering Program, Texas A&M University at Qatar, Engineering Building, P.O. Box 23874, Education City, Doha, Qatar.
[b] School of Mechanical Engineering, SASTRA University, Thanjavur - 613 401, Tamil Nadu, India.
[c] Swansea University, Bay Campus, Fabian Way, Swansea SA1 8EN, UK.
[d] Applied Mechanics and Systems Research Laboratory, Tunisia Polytechnic School, University of Carthage, B.P. 743, La Marsa 2078, Tunisia.
[e] Department of Mechanical Engineering, Tunis Higher National Engineering School, University of Tunis, Tunis 1008, Tunisia.
[f] Department of Mechanical Engineering, Texas A&M University, College Station, Texas 77843-3123, USA.

## Abstract

In this paper the torsional vibration of size-dependent viscoelastic nanorods embedded in an elastic medium with different boundary conditions is investigated. The novelty of this study consists of combining the nonlocal theory with the strain and velocity gradient theory to capture both softening and stiffening size-dependent behavior of the nanorods. The viscoelastic behavior is modelled using the so-called Kelvin–Voigt viscoelastic damping model.Three length-scale parameters are incorporated in this newly combined theory, namely, a nonlocal, a strain gradient, and a velocity gradient parameter. The governing equation of motion and its boundary conditions for the vibration analysis of nanorods are derived by employing Hamilton's principle. It is shown that the expressions of the classical stress and the stress gradient resultants are only defined for different values of the nonlocal and strain gradient parameters. The case where these are equal may seem to result in an inconsistency to the general equation of motion and the related non-classical boundary conditions. A rigorous investigation is conducted to prove that that the proposed solution is consistent with physics. Damped eigenvalue solutions are obtained both analytically and numerically using a Locally adaptive Differential Quadrature Method (LaDQM). Analytical results of linear free vibration response are obtained for various length-scales and compared with LaDQM numerical results.

**Keywords:** Torsional nanorod; nonlocal strain and velocity gradient theory; viscoelasticity; Kelvin–Voigt model; torsional vibration.

## 1 Introduction

Over the past few decades the demand of nanomaterials has been increasing enormously in various applications like actuators, sensors, microscopes, micro/nano electro mechanical systems (MEMS)/(NEMS). This is due to their superior properties such as high mechanical

[1]Corresponding author. Tel.: +974 4423 0674, e-mail: sami.el_borgi@qatar.tamu.edu (Sami El-Borgi).

strength and modulus, electrical conductivity, thermal conductivity etc. Micro/Nano-scaled structures are made of structural elements whose characteristic size (thickness, diameter, etc.) is in the order of micro/nanometers. These elements can be in the form of bars, rods, beams, plates or shell structures.

Two different modeling strategies have been adopted for modeling nano-structures, namely molecular dynamics (MD) simulation and continuum mechanics. The MD approach requires intense computational labor with a huge number of atoms. The continuum mechanics approach can also be used as an alternative, but it is incapable of predicting the size-dependent static and dynamic behavior of micro/nano-scaled structures. Recently, several non-classical continuum theories that incorporate the effect of material length scales have been proposed in the literature to predict the behavior of nanostructures. These include nonlocal, gradient elasticity and couple stress theories or a combination of these theories.

Unlike classical continuum mechanics, nonlocal theories assume that the stress at a point is not a function of the strain at that point but is a function of the strain in the entire domain containing the points [1]–[3]. These theories consider the body to be made of collection of particles modeled as mass points, take into account the inter-atomic long-range force and similar to classical elasticity do not consider the microstructure deformation mechanism. Nonlocal elastic models can only model nanostructures exhibiting softening behavior which indicates that "smaller is more compliant" [4]. Nonlocal theories have been used extensively in several studies including bending, buckling, vibrations, and wave propagation of nanoscale beams [5]–[7] and a review of these investigations can be found in [8].

On the other hand, the gradient elasticity theory stipulates that nanostructures should be modeled as atoms with higher-order deformation mechanism rather than collections of points, and the total stress should account for some additional strain gradient terms [9]–[11]. However, this theory does not consider the inter-atomic long-range force. Furthermore, gradient elasticity theory can only model nanostructures exhibiting hardening behavior which indicates that "smaller is stiffer" [4]. Therefore, it can be concluded that the nonlocal elasticity and gradient elasticity theories describe two completely different size-dependent nano/micro-mechanical properties of materials. Stated differently, combining both theories allows the modeling of nanostructures exhibiting at the same time hardening and softening behavior.

Experimental measurements on certain nanostructures revealed that the stiffness enhancement and softening effects may both be observed [12]. This indicates the need for a unique theory capable of capturing both size-dependent stiffness-softening and hardening phenomena. Recently, Lim et al. [13] introduced a nonlocal strain gradient theory which stipulates that the stress tensor should account for the effects of both nonlocal stress tensor and strain gradient stress tensor, thereby combining nonlocal and strain gradient theories into a unique theory. It was shown that the nonlocal strain gradient (NSG) theory exhibits a stiffness-softening and a stiffness-hardening effect when the nonlocal parameter is, respectively, larger and smaller than the material length scale parameter. Very recently, some researchers have exploited NSG theory to investigate the size-dependent mechanical behavior of nanorods [4, 14], nanobeams [18]–[24] and nanoplates [25]–[27].

Micro/nano rods subjected to torsional loads have been widely used in various types of MEMS/NEMS applications including torsional springs in NEMS oscillators [28], torsional micromirrors [29]–[30] and torsional microscanners [31]. Therefore, the accurate modeling of the static and dynamic torsional behavior of micro/nano bars seems to be essential in order to understand the mechanical behavior of these micro/nano systems. There have been few studies related to the size-dependent torsional vibration of nanotubes/nanorods. Most

of these studies utilized the differential nonlocal model and the following is a brief review. Lim et al. [32] obtained analytical solutions for the free torsional vibration of nanorods and concluded that the nonlocal parameter induces higher torsional stiffness which in turn increases the vibration frequency. In another study, Lim et al. [33] utilized the finite element method and the integral form of the nonlocal theory to study the torsional static and dynamic response of circular nanostructures. Demir and Civalek [34] developed a finite element model to investigate the torsional and axial vibration response of a microtube. Arda and Aydogdu [35] investigated analytically the static and free vibration response of a carbon nanotube (CNT) embedded in an elastic medium. Islam et al. [36] obtained analytical solutions for the wave propagation problem of an infinitely long torsional CNT rod. Li [37] developed two different nonlocal elasticity models to study the torsional vibration response of CNTs. Li and Hu [38] examined the free torsional vibration behavior of nanotubes made of a bi-directional functionally graded (FG) material. On the other hand, Kahrobaiyan et al. [39] used strain gradient theory to obtain closed-form analytical solutions for the static and free torsional vibration of a microbar.

Damping plays a vital role in the dynamic analysis of structures. Damping mechanisms are often complex and damping is considered either proportional external damping or internal damping based on viscoelastic models which include Kelvin–Voigt model and the Generalized Wiechert model [40]–[41] . Despite the tremendous interest in studying the dynamic behavior of nanosystems using size-dependent theories, there are, however, a limited number of investigations which accounted for damping. Lei et al. [42] investigated the dynamic behavior of nonlocal viscoelastic damped Timoshenko nanobeams using the Kelvin–Voigt viscoelastic model and velocity-dependent external damping. It was concluded that the external damping has an important effect on the natural frequencies. Karlicic et al. [43] studied the free longitudinal vibration of a nonlocal viscoelastic double-nanorod system. Polyzos et al. [44] used strain gradient theory of elasticity to study the torsional vibration of a nano-column assuming a viscoleastic material. Li et al. [21] investigated on the basis of NSGT and Kelvin–Voigt viscoelastic model the wave propagation problem of fluid-conveying viscoelastic single-walled carbon nanotubes (SWCNTs). Ebrahimi and Barati [45] studied the damped vibration characteristics of hygro-thermally affected FG viscoelastic nanobeams based on NSGT.

To improve material stiffness and fracture toughness, composite structures use nanomaterials reinforcement such as polymer/CNT nanocomposites (PCNTs) [46]. Thanks to their excellent properties, nanomaterials have been used along with matrices of many polymer resins for CNT-nanocomposites, such as CNT/Polypropylene [47], CNT/Nylon [48] and CNT/Polycarbonate [49]. This type of composite structures and especially the interaction of the nanomaterial with the surrounding elastic medium has attracted the interest of researchers. Three types of interaction models have been mainly utilized, including Winkler type [17, 35, 50], Pasternak type [51] and a combination of Winkler and Pasternak types [45].

From the above literature review, it can be concluded that the works related to torsional vibration of nanorods/nanotubes were either based on non-local elasticity theory or strain gradient theory and did not account for viscoelastic effects. To fill these gaps in the literature, the novelty of this paper consists of combining the nonlocal theory with the strain and velocity gradient theory to capture softening and stiffening size-dependent behavior to study, analytically and numerically, the torsional vibration of a viscoelastic nanorod embedded in an elastic medium. This theory involves three length-scale parameters, namely, a nonlocal, a strain gradient and a velocity gradient parameter denoted, respectively, $\mu_0$, $l_s$ and $l_k$. It

will be shown that the expressions of the classical stress and the stress gradient resultants are only defined when $\mu_0 \neq l_s$. The case $\mu_0 = l_s$ may seem to result in an inconsistency to the general equation of motion and the related non-classical boundary conditions. In fact, the expression of the stress gradient resultant may suggest an infinite value when $\mu_0 = l_s$ [52]. However, as an additional novelty of this work, it will be shown that calculating the limit of the stress gradient resultant is finite and, therefore, the proposed solution will not show any inconsistency.

The paper is arranged as follows. Section 2 describes the nonlocal strain gradient viscoelastic theory. The equation of motion of size-dependent torsional rods is derived in Section 3. The analytical solution of the vibration problem is established in Section 4. The formulation and solution for the particular case where $\hat{\mu}_0 = \hat{l}_s$ is outlined in Section 5. The numerical formulation using a Locally adaptive Differential Quadrature Method (LaDQM) is summarized in Section 6. Analytical and numerical results are presented and discussed in Section 7. Finally, concluding remarks are provided in Section 8.

## 2 Nonlocal strain gradient viscoelastic theory

The nonlocal strain gradient theory proposed by [13, 14] stipulates that the total stress tensor $\mathbf{t}$ accounts for both the nonlocal stress tensor $\sigma$ and the higher-order strain gradient nonlocal stress tensor $\nabla\sigma^{(1)}$, in which $\sigma^{(1)}$ is the higher-order nonlocal stress tensor. Stated differently, the total stress at a reference point $\mathbf{x}$ depends not only on the strain $\boldsymbol{\varepsilon}$ and its gradient at that location but on the strains and their gradients at all other points within the domain $V$. This can be written mathematically as

$$\mathbf{t} = \sigma - \nabla\sigma^{(1)} \tag{1}$$

where $\nabla$ is the gradient operator and $\sigma$ and $\sigma^{(1)}$ are given by

$$\sigma = \int_V \alpha_0 \left(\left|\mathbf{x}-\mathbf{x}'\right|, e_0 a\right) \mathbf{C} : \varepsilon\left(\mathbf{x}'\right)\ dV \tag{2a}$$

$$\sigma^{(1)} = l_s^2 \int_V \alpha_1 \left(\left|\mathbf{x}-\mathbf{x}'\right|, e_1 a\right) \mathbf{C} : \nabla\varepsilon\left(\mathbf{x}'\right)\ dV \tag{2b}$$

in which $\varepsilon(\mathbf{x}')$ and $\nabla\varepsilon(\mathbf{x}')$ are, respectively, the classical strain tensor and its gradient at point $\mathbf{x}'$, $\mathbf{C}$ is the fourth-order elasticity tensor, $l_s$ is the strain gradient length-scale parameter, $e_0 a$ and $e_1 a$ are nonlocal parameters representing the significance of the interatomic long-range force, and $\alpha_0$ and $\alpha_1$ are kernel functions.

In view of the difficulty in using the integral constitutive relations (1), (2a) and (2b), Eringen [2] proposed an equivalent differential model. Thus, assuming $e_0 a = e_1 a = e a = \mu_0$ and for a suitable choice of the kernel functions $\alpha_0$ and $\alpha_1$, Eqs. (2a) and (2b) become

$$\left(1-\mu_0^2\nabla^2\right)\boldsymbol{\sigma} = \mathbf{C} : \boldsymbol{\varepsilon} \tag{3a}$$

$$\left(1-\mu_0^2\nabla^2\right)\boldsymbol{\sigma}^{(1)} = l_s^2 \mathbf{C} : \nabla\boldsymbol{\varepsilon} \tag{3b}$$

where $\nabla^2$ is the Laplacian operator. Substituting (3a) and (3b) into (1) yields

$$\left(1-\mu_0^2\nabla^2\right)\mathbf{t} = \left(1-l_s^2\nabla^2\right)\mathbf{C} : \boldsymbol{\varepsilon} \tag{4}$$

Furthermore, for a torsional rod-type structure defined in a cylindrical coordinate system $(r, \theta, x)$ where $r$ is the radial axis, $\theta$ is the angular axis and $x$ is the longitudinal axis, we

assume the size-dependency is only accounted for in the longitudinal direction and neglected in the other directions. Therefore, Eq. (4) can be reduced to the following:

$$\left(1-\mu_0^2\frac{\partial^2}{\partial x^2}\right)t_{r\theta}=\left(1-l_s^2\frac{\partial^2}{\partial x^2}\right)G\varepsilon_{r\theta} \tag{5}$$

where $\nabla^2$ was replaced by $\partial^2/\partial x^2$, $t_{r\theta}$ is the total shear stress, $\varepsilon_{r\theta}$ is the shear strain and $G$ is the rod's modulus of rigidity. This model combines Eringen's nonlocal elasticity theory and strain gradient theory to obtain the Nonlocal Strain Gradient (NSG) theory. The following limiting cases correspond to existing theories:

- Setting $l_s = 0$, Eq. (5) reduces to $\left(1-\mu_0^2\frac{\partial^2}{\partial x^2}\right)t_{r\theta} = G\varepsilon_{r\theta}$ which corresponds to Eringen's nonlocal theory.
- Setting $\mu_0 = 0$, Eq. (5) simplifies to $t_{r\theta} = \left(1-l_s^2\frac{\partial^2}{\partial x^2}\right)G\varepsilon_{r\theta}$ which is the strain gradient theory.

Viscoelastic damping may be added to the constitutive relation (5) by incorporating the Kelvin–Voigt viscoelastic model [53] which then becomes

$$\left(1-\mu_0^2\frac{\partial^2}{\partial x^2}\right)t_{r\theta}=\left(1-l_s^2\frac{\partial^2}{\partial x^2}\right)G\left(\varepsilon_{r\theta}+g\dot{\varepsilon}_{r\theta}\right)=\left(1+g\frac{\partial}{\partial t}\right)\left(1-l_s^2\frac{\partial^2}{\partial x^2}\right)G\varepsilon_{r\theta} \tag{6}$$

where $g$ is the damping coefficient and $\dot{\varepsilon}_{r\theta}=\partial\varepsilon_{r\theta}/\partial t$ is the rate of shear strain with respect to the time variable $t$. For subsequent derivations, it will be useful to rewrite Eqs. (1), (3a) and (3b) for the case of torsional rods with viscoelastic damping as

$$t_{r\theta}=\sigma_{r\theta}-\frac{\partial\sigma_{r\theta}^{(1)}}{\partial x} \tag{7}$$

$$\left(1-\mu_0^2\frac{\partial^2}{\partial x^2}\right)\sigma_{r\theta}=\left(1+g\frac{\partial}{\partial t}\right)G\varepsilon_{r\theta} \tag{8}$$

$$\left(1-\mu_0^2\frac{\partial^2}{\partial x^2}\right)\sigma_{r\theta x}^{(1)}=l_s^2\left(1+g\frac{\partial}{\partial t}\right)G\frac{\partial\varepsilon_{r\theta}}{\partial x} \tag{9}$$

Here $\sigma_{r\theta}$ is the nonlocal shear stress and $\sigma_{r\theta x}^{(1)}$ is the higher-order nonlocal shear stress.

## 3 Equations of motion of size-dependent rods

The displacement field in a rod of volume $V$, length $L$ and cross-sectional area $A$ takes the following form:

$$\theta_1=\theta\left(x,t\right),\quad \theta_2=0,\quad \theta_3=0 \tag{10}$$

Here $\theta_1$, $\theta_2$ and $\theta_3$ denote the time dependent rotations about the $x$, $y$ and $z$ directions, respectively. The shear strain of a torsional rod can be written as

$$\varepsilon_{r\theta}=r\frac{\partial\theta}{\partial x} \tag{11}$$

and its gradient with respect to $x$ is

$$\varepsilon_{r\theta,x}=r\frac{\partial^2\theta}{\partial x^2} \tag{12}$$

The strain energy, $U$, after integrating by parts and using Eq. (11) and (12), is then

$$\begin{aligned} U &= \int_V \left(\sigma_{r\theta}\varepsilon_{r\theta} + \sigma^{(1)}_{r\theta x}\varepsilon_{r\theta,x}\right) dV \\ &= \int_V \left(\sigma_{r\theta}\varepsilon_{r\theta} - \nabla\sigma^{(1)}_{r\theta x}\varepsilon_{r\theta}\right) dV + \left[\int_A \sigma^{(1)}_{r\theta x}\varepsilon_{r\theta} dA\right]_0^L \\ &= \int_0^L \int_A t_{r\theta}\varepsilon_{r\theta} dA dx + \left[\int_A \sigma^{(1)}_{r\theta x}\varepsilon_{r\theta} dA\right]_0^L \\ &= \int_0^L T\frac{\partial\theta}{\partial x} dx + \left[T^{(1)}\frac{\partial\theta}{\partial x}\right]_0^L \end{aligned} \tag{13}$$

where $T$ and $T^{(1)}$ are the stress resultants of, respectively, the total stress and the higher-order stress which are given by

$$T = \int_A r t_{r\theta} dA \tag{14a}$$

$$T^{(1)} = \int_A r\sigma^{(1)}_{r\theta x} dA \tag{14b}$$

and the stress resultant of the classical stress $T^{(0)}$ can be defined as

$$T^{(0)} = \int_A r\sigma_{r\theta} dA \tag{15}$$

The stress resultants $T$, $T^{(0)}$ and $T^{(1)}$ can be related by multiplying both sides of Eq. (7) by $r$ and integrating over the cross-sectional area of the rod, to give

$$T = T^{(0)} - \frac{\partial T^{(1)}}{\partial x} \tag{16}$$

$T^{(0)}$ and $T^{(1)}$ are, respectively, solutions of the following ordinary differential equations which are obtained by multiplying both sides of Eqs. (8) and (9) by $r$, integrating over the cross sectional area of the rod and substituting Eq. (11) into the resulting equations:

$$T^{(0)} - \mu_0^2\frac{\partial^2 T^{(0)}}{\partial x^2} = \left(1 + g\frac{\partial}{\partial t}\right) GJ\frac{\partial\theta}{\partial x} \tag{17}$$

$$T^{(1)} - \mu_0^2\frac{\partial^2 T^{(1)}}{\partial x^2} = \left(1 + g\frac{\partial}{\partial t}\right) l_s^2 GJ\frac{\partial^2\theta}{\partial x^2} \tag{18}$$

By observing the above equations, it can be concluded that $T^{(0)}$ and $T^{(1)}$ are related as follows:

$$T^{(1)} = l_s^2\frac{\partial T^{(0)}}{\partial x} \tag{19}$$

Substituting Eq. (19) into Eq. (16) gives an expression of $T$ in terms of $T^{(0)}$ as

$$T = T^{(0)} - l_s^2\frac{\partial^2 T^{(0)}}{\partial x^2} \tag{20}$$

Solving the above equation for $\frac{\partial^2 T^{(0)}}{\partial x^2}$ and substituting the above expression in Eq. (17) yields the following expression for $T^{(0)}$ in terms of $T$:

$$T^{(0)} = \left(\frac{\mu_0^2}{\mu_0^2 - l_s^2}\right) T - \left(\frac{l_s^2}{\mu_0^2 - l_s^2}\right) \left(1 + g\frac{\partial}{\partial t}\right) GJ \frac{\partial \theta}{\partial x} \tag{21}$$

Considering the torsional motion of the rod and its velocity gradient, the kinetic energy, $K$, can be written as

$$K = \frac{1}{2}\rho J \int_0^L \left(\frac{\partial \theta}{\partial t}\right)^2 dx + \frac{1}{2}\rho J l_k^2 \int_0^L \left(\frac{\partial^2 \theta}{\partial x \partial t}\right)^2 dx \tag{22}$$

where $\rho$ is the density of the rod and $l_k$ is the kinetic material length-scale parameter associated with the velocity gradient.

The surrounding medium is assumed to be a Winkler type model [50], where $k_{EM}$ is the linear torsional stiffness. Then, the external work done by the surrounding medium is

$$W = -\int_0^L k_{EM} \theta^2 d\theta \tag{23}$$

The equations of motion are obtained by applying Hamilton's Principle and the fundamental lemma of calculus variations. After integration by parts with respect to $t$ as well as $x$, and setting the initial conditions to zero, the following equation of motion can be derived:

$$-\rho J \frac{\partial^2 \theta}{\partial t^2} + \rho J l_k^2 \frac{\partial^4 \theta}{\partial x^2 \partial t^2} + \frac{\partial T}{\partial x} - k_{EM}\theta = 0 \tag{24}$$

Substituting Eqs. (17) and (18) into Eq. (16) yields

$$T = \mu_0^2 \frac{\partial^2 T}{\partial x^2} + \left(1 + g\frac{\partial}{\partial t}\right)\left(1 - l_s^2 \frac{\partial^2}{\partial x^2}\right) GJ \frac{\partial \theta}{\partial x} \tag{25}$$

Differentiating the equation of motion, Eq. (24), with respect to $x$ and substituting $\frac{\partial^2 T}{\partial x^2}$ into Eq. (25) gives the expression of $T$ in terms of the rotation as

$$\begin{aligned} T = GJ\left(\frac{\partial \theta}{\partial x} + g\frac{\partial^2 \theta}{\partial x \partial t}\right) - GJ l_s^2 \left(\frac{\partial^3 \theta}{\partial x^3} + g\frac{\partial^4 \theta}{\partial x^3 \partial t}\right) + \\ \mu_0^2 \rho J \left(\frac{\partial^3 \theta}{\partial x \partial t^2} - l_k^2 \frac{\partial^5 \theta}{\partial x^3 \partial t^2}\right) + \mu_0^2 k_{EM} \frac{\partial \theta}{\partial x} \end{aligned} \tag{26}$$

Furthermore, differentiating this expression for $T$ with respect to $x$ and substituting into Eq. (24) gives the equation of motion in terms of the rotation as

$$\begin{aligned} \rho J \left[-\frac{\partial^2 \theta}{\partial t^2} + l_k^2 \frac{\partial^4 \theta}{\partial x^2 \partial t^2} + \mu_0^2 \left(\frac{\partial^4 \theta}{\partial x^2 \partial t^2} - l_k^2 \frac{\partial^6 \theta}{\partial x^4 \partial t^2}\right)\right] + \\ GJ\left[\frac{\partial^2 \theta}{\partial x^2} + g\frac{\partial^3 \theta}{\partial x^2 \partial t} - l_s^2 \left(\frac{\partial^4 \theta}{\partial x^4} + g\frac{\partial^5 \theta}{\partial x^4 \partial t}\right)\right] - k_{EM}\left(\theta - \mu_0^2 \frac{\partial^2 \theta}{\partial x^2}\right) = 0 \end{aligned} \tag{27}$$

This governing equation of motion for $\theta$ is subjected to the following classical and non-classical boundary conditions specified at each of the ends $x = 0$ and $x = L$:

$$T = 0 \quad \text{or} \quad \theta = 0 \tag{28}$$

$$T^{(1)} = 0 \quad \text{or} \quad \frac{\partial \theta}{\partial x} = 0 \tag{29}$$

The stress resultants $T$, is given by Eq. (26), however, an expression for the higher order stress $T^{(1)}$ needs to be obtained.

Substituting the expression of $T$ from Eq. (26) into Eq. (21) gives the stress resultant of the classical stress $T^{(0)}$, defined in Eq. (15), in terms of the rotation as

$$\begin{aligned} T^{(0)} = \frac{\mu_0^4}{\mu_0^2 - l_s^2}\left[k_{EM}\frac{\partial \theta}{\partial x} + \rho J\left(\frac{\partial^3 \theta}{\partial x \partial t^2} - l_k^2 \frac{\partial^5 \theta}{\partial x^3 \partial t^2}\right)\right] - \\ GJ\frac{\mu_0^2 l_s^2}{\mu_0^2 - l_s^2}\left(\frac{\partial^3 \theta}{\partial x^3} + g\frac{\partial^4 \theta}{\partial x^3 \partial t}\right) + GJ\left(\frac{\partial \theta}{\partial x} + g\frac{\partial^2 \theta}{\partial x \partial t}\right) \end{aligned} \tag{30}$$

Likewise, substituting this expression for $T^{(0)}$ into Eq. (19) gives the resultant of the stress gradient $T^{(1)}$, defined in (14b), in terms of the rotation as

$$\begin{aligned} T^{(1)} = \frac{\mu_0^4 l_s^2}{\mu_0^2 - l_s^2}\left[k_{EM}\frac{\partial^2 \theta}{\partial x^2} + \rho J\left(\frac{\partial^4 \theta}{\partial x^2 \partial t^2} - l_k^2 \frac{\partial^6 \theta}{\partial x^4 \partial t^2}\right)\right] - \\ GJ\frac{\mu_0^2 l_s^4}{\mu_0^2 - l_s^2}\left(\frac{\partial^4 \theta}{\partial x^4} + g\frac{\partial^5 \theta}{\partial x^4 \partial t}\right) + GJ l_s^2\left(\frac{\partial^2 \theta}{\partial x^2} + g\frac{\partial^3 \theta}{\partial x^2 \partial t}\right) \end{aligned} \tag{31}$$

Using the following non-dimensional parameters:

$$\begin{aligned} &\xi = \frac{x}{L}, \quad \tau = \frac{t}{L}\sqrt{\frac{G}{\rho}}, \quad \theta(x,t) = \theta(\xi,\tau) \\ &\hat{\mu_0} = \frac{\mu_0}{L}, \quad \hat{g} = \frac{g}{L}\sqrt{\frac{G}{\rho}}, \quad \hat{l}_s = \frac{l_s}{L}, \quad \hat{l}_k = \frac{l_k}{L}, \quad \hat{k}_{EM} = \frac{k_{EM} L^2}{GJ}, \end{aligned} \tag{32}$$

the governing equations, Eq. (27), along with the associated boundary conditions, Eqs. (28) and (29), can be written in non-dimensional form as

$$\begin{aligned} -\frac{\partial^2 \theta}{\partial \tau^2} + \hat{l}_k^2 \frac{\partial^4 \theta}{\partial \xi^2 \partial \tau^2} + \hat{\mu}_0^2\left(\frac{\partial^4 \theta}{\partial \xi^2 \partial \tau^2} - \hat{l}_k^2 \frac{\partial^6 \theta}{\partial \xi^4 \partial \tau^2}\right) + \\ \frac{\partial^2 \theta}{\partial \xi^2} + \hat{g}\frac{\partial^3 \theta}{\partial \xi^2 \partial \tau} - \hat{l}_s^2\left(\frac{\partial^4 \theta}{\partial \xi^4} + \hat{g}\frac{\partial^5 \theta}{\partial \xi^4 \partial \tau}\right) - \hat{k}_{EM}\left(\theta - \hat{\mu}_0^2 \frac{\partial^2 \theta}{\partial \xi^2}\right) = 0 \end{aligned} \tag{33}$$

subject to the boundary conditions specified at each of the ends $\xi = 0$ and $\xi = 1$

$$\hat{T} = 0 \quad \text{or} \quad \theta = 0 \tag{34a}$$

$$\hat{T}^{(1)} = 0 \quad \text{or} \quad \frac{\partial \theta}{\partial \xi} = 0 \tag{34b}$$

The non-dimensional expressions of the stress resultants $T$, $T^{(0)}$ and $T^{(1)}$ can be written as

$$\begin{aligned} \hat{T} = \hat{\mu}_0^2 k_{EM}\frac{\partial \theta}{\partial \xi} + \hat{\mu}_0^2\left(\frac{\partial^3 \theta}{\partial \xi \partial \tau^2} - \hat{l}_k^2 \frac{\partial^5 \theta}{\partial \xi^3 \partial \tau^2}\right) - \\ \hat{l}_s^2\left(\frac{\partial^3 \theta}{\partial \xi^3} + \hat{g}\frac{\partial^4 \theta}{\partial \xi^3 \partial \tau}\right) + \left(\frac{\partial \theta}{\partial \xi} + \hat{g}\frac{\partial^2 \theta}{\partial \xi \partial \tau}\right) \end{aligned} \tag{35}$$

$$\hat{T}^{(0)} = \frac{\hat{\mu}_0^4}{\hat{\mu}_0^2 - \hat{l}_s^2}\left[k_{EM}\frac{\partial\theta}{\partial\xi} + \left(\frac{\partial^3\theta}{\partial\xi\partial\tau^2} - \hat{l}_k^2\frac{\partial^5\theta}{\partial\xi^3\partial\tau^2}\right)\right] - \frac{\hat{\mu}_0^2\hat{l}_s^2}{\hat{\mu}_0^2 - \hat{l}_s^2}\left(\frac{\partial^3\theta}{\partial\xi^3} + \hat{g}\frac{\partial^4\theta}{\partial\xi^3\partial\tau}\right) + \left(\frac{\partial\theta}{\partial x} + \hat{g}\frac{\partial^2\theta}{\partial\xi\partial\tau}\right) \tag{36}$$

$$\hat{T}^{(1)} = \frac{\hat{\mu}_0^4}{\hat{\mu}_0^2 - \hat{l}_s^2}\left(\hat{k}_{EM}\frac{\partial^2\theta}{\partial\xi^2} + \frac{\partial^4\theta}{\partial\xi^2\partial\tau^2} - \hat{l}_k^2\frac{\partial^6\theta}{\partial\xi^4\partial\tau^2}\right) - \frac{\hat{\mu}_0^2 l_s^2}{\hat{\mu}_0^2 - \hat{l}_s^2}\left(\frac{\partial^4\theta}{\partial\xi^4} + \hat{g}\frac{\partial^5\theta}{\partial\xi^4\partial\tau}\right) + \hat{l}_s^2\left(\frac{\partial^2\theta}{\partial\xi^2} + \hat{g}\frac{\partial^3\theta}{\partial\xi^2\partial\tau}\right) \tag{37}$$

## 4 Analytical solution of the vibration problem

The solution of the non-dimensional PDE in Eq. (33) proceeds in the usual way by assuming a separable solution of the form $\theta(\xi,\tau) = \phi(\xi)e^{st}$. The resulting ODE for $\phi(\xi)$ is then

$$\left(s^2\hat{l}_k^2\hat{\mu}_0^2 + \hat{g}s\hat{l}_s^2 + \hat{l}_s^2\right)\frac{d^4\phi}{d\xi^4} - \left(s^2\hat{l}_k^2 + s^2\hat{\mu}_0^2 + \hat{k}_{EM}\hat{\mu}_0^2 + \hat{g}s + 1\right)\frac{d^2\phi}{d\xi^2} + \left(s^2 + \hat{k}_{EM}\right)\phi(\xi) = 0 \tag{38}$$

or equivalently

$$\alpha(s)\frac{\mathrm{d}^4\phi}{\mathrm{d}\xi^4} + \beta(s)\frac{\mathrm{d}^2\phi}{\mathrm{d}\xi^2} + \gamma(s)\phi = 0 \tag{39}$$

where

$$\begin{aligned}\alpha(s) &= s^2\hat{l}_k^2\hat{\mu}_0^2 + \hat{g}s\hat{l}_s^2 + \hat{l}_s^2\\ \beta(s) &= -\left(s^2\hat{l}_k^2 + s^2\hat{\mu}_0^2 + \hat{k}_{EM}\hat{\mu}_0^2 + \hat{g}s + 1\right)\\ \gamma(s) &= s^2 + \hat{k}_{EM}\end{aligned} \tag{40}$$

Since Eq. (39) is a linear ODE for fixed $s$, the solution is of the form $\phi(\xi) = Ce^{\lambda\xi}$, which gives a quadratic equation in $\lambda^2$ as

$$\alpha(s)\lambda^4 + \beta(s)\lambda^2 + \gamma(s) = 0 \tag{41}$$

which has four solutions $\lambda_i(s)$ for $i = 1,\ldots,4$. Note that we may assume that $\lambda_3 = -\lambda_1$ and $\lambda_4 = -\lambda_2$. The general solution for the mode shape is

$$\phi(\xi) = C_1e^{\lambda_1\xi} + C_2e^{\lambda_2\xi} + C_3e^{\lambda_3\xi} + C_4e^{\lambda_4\xi} \tag{42}$$

for some constants $C_i$. Note that Eq. (42) may also be written in terms of hyberbolic or trignometric functions, which can make the solution easier for some boundary conditions.

The four boundary conditions required for the fourth order differential equation allows the constants $C_i$ and the eigenvalues, $s$, to be calculated. Note that for the free vibration problem the amplitude of the mode shape is arbitrary, which means that there are essentially only three independent unknown $C_i$ constants. Each boundary condition gives a linear

equation in the $C_i$ constants. Thus, for example,

$$\begin{aligned}
\phi(0) = 0 \quad &\text{implies} \quad C_1 + C_2 + C_3 + C_4 = 0 \\
\phi(1) = 0 \quad &\text{implies} \quad C_1 e^{\lambda_1} + C_2 e^{\lambda_2} + C_3 e^{\lambda_3} + C_4 e^{\lambda_4} \\
\frac{\mathrm{d}\phi}{\mathrm{d}\xi}(0) = 0 \quad &\text{implies} \quad \lambda_1 C_1 + \lambda_2 C_2 + \lambda_3 C_3 + \lambda_4 C_4 = 0 \\
\hat{T}(0) = 0 \quad &\text{implies} \quad C_1 \left( \lambda_1 \left(1 + \hat{g} s\right) \left(1 - \hat{l}_s^2 \lambda_1^2\right) + \hat{\mu}_0^2 \lambda_1 s^2 \left(1 - \hat{l}_k^2 \lambda_1^2\right) + \hat{\mu}_0^2 \hat{k}_{EM} \lambda_1 \right) \\
&\qquad + C_2 \left(\ldots\right) + C_3 \left(\ldots\right) + C_4 \left(\ldots\right) = 0
\end{aligned} \tag{43}$$

Note that the $\lambda_i$ depend on $s$. For the last example boundary condition, $\hat{T}(0) = 0$, is obtained by substituting Eq. (42) into Eq. (35). The coefficients for $C_2$, $C_3$ and $C_4$ are similar to the coefficient for $C_1$ with $\lambda_1$ replaced by the corresponding $\lambda_i$. The $\hat{T}^{(1)}$ boundary condition may be obtained in a similar way using Eq. (37).

The four boundary conditions give four linear homogeneous equations in the $C_i$, and for a non-trivial solution the determinant of the coefficient matrix, which only depends on $s$, must be zero. This gives an equation for $s$, although often this equation is highly nonlinear and difficult to solve analytically. Even obtaining all of the solutions numerically is difficult, and would be helped by reasonable initial estimates, perhaps from the undamped case.

Three sets of boundary conditions are now considered for the torsional rod, where the mode shapes may be determined directly. These special cases are (a) Clamped Forcing-Clamped Forcing (CF-CF), (b) Clamped Forcing - Free Strained (CF-FS), (c) Free Strained - Free Strained (FS-FS). Table 1 gives the mode shapes, where $C_n$ is an arbitrary constant, and it is straightforward to verify that these functions satisfy the given boundary conditions by directly substituting into the expressions for $\hat{T}$ and $\hat{T}^{(1)}$ given earlier. Here we will assume that $\hat{\mu}_0 \neq \hat{l}_s$ for the CF-CF and FS-FS cases, since $\hat{T}^{(1)}$ given by Eq. (37) is not defined when $\hat{\mu}_0 = \hat{l}_s$; the solution for $\hat{\mu}_0 = \hat{l}_s$ is considered in detail in the next section. The mode shapes in Table 1 give direct expressions for $\lambda_i$, which may be substituted into Eq. (41), using the expressions for $\alpha$, $\beta$ and $\gamma$ from Eq. (40), to give the following quadratic equation for $s$:

$$as^2 + bs + c = 0 \tag{44}$$

where the expressions of $a$, $b$ and $c$ for the three boundary conditions CF-CF, CF-FS and FS-FS are given in Table 2. This quadratic equation is easily solved to obtain the solutions for $s$, and hence the corresponding natural frequencies and damping ratios.

For each set of boundary conditions, solutions for particular cases of interest can be obtained, namely, local undamped ($\hat{\mu}_0 = \hat{l}_k = \hat{l}_s = \hat{g} = 0$), local damped ($\hat{\mu}_0 = \hat{l}_k = \hat{l}_s = 0$) and asymptotic cases. In the last case, the asymptotic frequencies are obtained by taking the asymptotic expansion of Eq. (44) when $n \to \infty$ and then keeping the leading terms of order $n^4$ before solving for $s$ to give the natural frequencies and damping ratios. All these solutions are summarized in Table 3. It is worth noting that the solutions for the CF-CF and FS-FS boundary conditions are identical because the ordinary differential equation (39) contains $\frac{\mathrm{d}^4\phi}{\mathrm{d}\xi^4}$ and $\frac{\mathrm{d}^2\phi}{\mathrm{d}\xi^2}$ and the mode shapes for these boundary conditions are, respectively, given by $\sin(n\pi\xi)$ and $\cos(n\pi\xi)$.

Table 1: Boundary conditions (BC) and modeshapes for the analytical solution.

| BC | BC Equations | Mode shape | $\lambda_n^2$ |
|---|---|---|---|
| CF-CF | $\phi(0)=0,\ \hat{T}^{(1)}(0)=0,$<br>$\phi(1)=0,\ \hat{T}^{(1)}(1)=0$ | $\phi(\xi)=C_n\sin(n\pi\xi)$<br>$n\geq 1$ | $-n^2\pi^2$ |
| CF-FS | $\phi(0)=0,\ \hat{T}^{(1)}(0)=0,$<br>$\frac{d\phi(1)}{d\xi}=0,\ \hat{T}(1)=0$ | $\phi(\xi)=C_n\sin\left(\frac{2n-1}{2}\pi\xi\right)$<br>$n\geq 1$ | $-\left(n-\frac{1}{2}\right)^2\pi^2$ |
| FS-FS | $\frac{d\phi(0)}{d\xi}=0,\ \hat{T}(0)=0,$<br>$\frac{d\phi(1)}{d\xi}=0,\ \hat{T}(1)=0$ | $\phi(\xi)=C_n\cos(n\pi\xi)$<br>$n\geq 0$ | $-n^2\pi^2$ |

Table 2: Expressions of the constants of the characteristic polynomial asociated with the analytical solution.

| Case | Polynomial constants | | |
|---|---|---|---|
| CF-CF & FS-FS | $a$ | $=$ | $n^4\pi^4\hat{l}_k^2\hat{\mu}_0^2+n^2\pi^2\hat{l}_k^2+n^2\pi^2\hat{\mu}_0^2+1$ |
| | $b$ | $=$ | $\hat{g}n^4\pi^4\hat{l}_s^2+\hat{g}n^2\pi^2$ |
| | $c$ | $=$ | $n^4\pi^4\hat{l}_s^2+n^2\pi^2\hat{k}_{EM}\hat{\mu}_0^2+n^2\pi^2+\hat{k}_{EM}$ |
| CF-FS | $a$ | $=$ | $\left(n-\frac{1}{2}\right)^4\pi^4\hat{l}_k^2\hat{\mu}_0^2+\left(n-\frac{1}{2}\right)^2\pi^2\left(\hat{l}_k^2+\hat{\mu}_0^2\right)+1$ |
| | $b$ | $=$ | $\hat{g}\left(n-\frac{1}{2}\right)^4\pi^4\hat{l}_s^2+\hat{g}\left(n-\frac{1}{2}\right)^2\pi^2$ |
| | $c$ | $=$ | $\left(n-\frac{1}{2}\right)^4\pi^4\hat{l}_s^2+\left(n-\frac{1}{2}\right)^2\pi^2\left(\hat{k}_{EM}\hat{\mu}_0^2+1\right)+\hat{k}_{EM}$ |

Table 3: Eigenvalues for particular cases of the analytical solution.

| | CF-CF and FS-FS | CS-FS |
|---|---|---|
| Local undamped case<br>$\hat{\mu}_0 = \hat{l}_k = \hat{l}_s = \hat{g} = 0$ | $\pm i\sqrt{n^2\pi^2 + \hat{k}_{EM}}$ | $\pm i\sqrt{\kappa + \hat{k}_{EM}}$ |
| Local damped case<br>$\hat{\mu}_0 = \hat{l}_k = \hat{l}_s = 0$ | $-\frac{1}{2}\hat{g}\pi^2 n^2 \pm \sqrt{\frac{1}{4}\hat{g}^2\pi^4 n^4 - \pi^2 n^2 - \hat{k}_{EM}}$ | $-\frac{1}{2}\hat{g}\kappa \mp \sqrt{\frac{1}{4}\hat{g}^2\kappa^2 - \kappa - \hat{k}_{EM}}$ |
| Asymptotic case<br>$n \to \infty$ | $\frac{1}{2}\frac{\hat{l}_s}{\hat{l}_k^2\hat{\mu}_0^2}\left(-\hat{g}\hat{l}_s \pm \sqrt{\hat{g}^2\hat{l}_s^2 - 4\hat{l}_k^2\hat{\mu}_0^2}\right)$ | Same as CF-CF case |

where $i = \sqrt{-1}$ and $\kappa = \left(n - \frac{1}{2}\right)^2 \pi^2$

## 5 Formulation and solution for particular case $\hat{\mu}_0 = \hat{l}_s$

The partial differential equation for $\theta$ given in Eq. (33) is well defined for $\hat{\mu}_0 = \hat{l}_s$, and is given by

$$-\frac{\partial^2\theta}{\partial\tau^2} + \hat{l}_k^2\frac{\partial^4\theta}{\partial\xi^2\partial\tau^2} + \frac{\partial^2\theta}{\partial\xi^2} + \hat{g}\frac{\partial^3\theta}{\partial\xi^2\partial\tau} - \hat{k}_{EM}\theta + \hat{\mu}_0^2\left(\frac{\partial^4\theta}{\partial\xi^2\partial\tau^2} - \hat{l}_k^2\frac{\partial^6\theta}{\partial\xi^4\partial\tau^2} - \frac{\partial^4\theta}{\partial\xi^4} - \hat{g}\frac{\partial^5\theta}{\partial\xi^4\partial\tau} + \hat{k}_{EM}\frac{\partial^2\theta}{\partial\xi^2}\right) = 0 \tag{45}$$

This differential equation can be conveniently written as

$$\left(1 - \hat{\mu}_0^2\frac{\partial^2}{\partial\xi^2}\right)\mathcal{L}(\theta) = 0 \tag{46}$$

where

$$\mathcal{L}(\theta) = -\frac{\partial^2\theta}{\partial\tau^2} + \hat{l}_k^2\frac{\partial^4\theta}{\partial\xi^2\partial\tau^2} + \frac{\partial^2\theta}{\partial\xi^2} + \hat{g}\frac{\partial^3\theta}{\partial\xi^2\partial\tau} - \hat{k}_{EM}\theta \tag{47}$$

However, the expressions for the classical stress and the stress gradient resultants given in non-dimensional form in Eqs. (36) and (37) are not defined when $\hat{\mu}_0 = \hat{l}_s$. In this case, using Eqs. (17) and (20), the total stress resultant given by Eq. (35) degenerates to

$$\hat{T} = \left(\frac{\partial\theta}{\partial\xi} + \hat{g}\frac{\partial^2\theta}{\partial\xi\partial\tau}\right) \tag{48}$$

Consider now the calculation of the higher order stress $\hat{T}^{(1)}$ when $\hat{\mu}_0 = \hat{l}_s$. This cannot be calculated from Eq. (37), because the denominator term $\hat{\mu}_0^2 - \hat{l}_s^2$ is zero. To determine $\hat{T}^{(1)}$ we have to consider the solution for $\theta$ and integrate the non-dimensional form of Eq. (18) directly. The solution proceeds in the usual way by assuming a separable solution of the form $\theta(\xi,\tau) = \phi(\xi)e^{st}$, which gives a linear fourth order ODE for $\phi(\xi)$. The general solution is

$$\phi(\xi) = C_1 e^{\lambda(s)\xi} + C_2 e^{-\lambda(s)\xi} + C_3 e^{\hat{\mu}_0\xi} + C_4 e^{-\hat{\mu}_0\xi} \tag{49}$$

where $\lambda$ is obtained from

$$\lambda^2\left(\hat{l}_k^2 s^2 + 1 + \hat{g}s\right) - s^2 - \hat{k}_{EM} = 0 \tag{50}$$

Table 4: Expressions of the constants of the characteristic polynomial and the corresponding eigenvalues for the particular case $\hat{\mu}_0 = \hat{l}_s$.

| Case | Polynomial constants | Eigenvalue solution |
|---|---|---|
| CF-CF & FS-FS | $a = n^2\pi^2 {l_k}^2 + 1$<br>$b = g n^2 \pi^2$<br>$c = n^2\pi^2 + k_{EM}$ | $\frac{-b \pm \sqrt{b^2 - 4ac}}{2a}$ |
| CF-FS | $a = \left(n - \frac{1}{2}\right)^2 \pi^2 l_k^2 + 1$<br>$b = g\left(n - \frac{1}{2}\right)^2 \pi^2$<br>$c = \left(n - \frac{1}{2}\right)^2 \pi^2 + k_{EM}$ | $\frac{-b \pm \sqrt{b^2 - 4ac}}{2a}$ |

The key issue in integrating Eq. (18) is now apparent in the treatment of the $e^{\pm\hat{\mu}_0\xi}$ terms. However the integration is easily performed by introducing $\xi e^{\pm\hat{\mu}_0\xi}$ terms to give

$$\hat{T}^{(1)}(\xi) = (1 + \hat{g}s)\,\hat{\mu}_0^2 \left( \frac{C_1 e^{\lambda\xi} + C_2 e^{-\lambda\xi}}{\lambda^2 - \hat{\mu}_0^2} - \frac{C_3 \xi e^{\hat{\mu}_0\xi} - C_4 \xi e^{-\hat{\mu}_0\xi}}{2\hat{\mu}_0^3} \right) \tag{51}$$

This gives the relationship between the $C_i$ coefficients to implement boundary conditions for $\hat{T}^{(1)}$ when $\hat{\mu}_0 = \hat{l}_s$.

For the three boundary conditions CF-CF, CF-FS and FS-FS, and using the same mode shapes as in the general case, the eigenvalues $s$, are the solutions of the quadratic equation in Eq. (44), where expressions for $a$, $b$ and $c$ are given in Table 4.

To show the consistency of the solution, Figs. 1 and 2 illustrate the variation of the first three frequencies and damping ratios as a function of $\Delta\mu l_s = \hat{l}_s - \hat{\mu}_0$ for CF-CF/FS-FS and CF-FS boundary conditions, respectively. When $\hat{\mu}_0$ is close to $\hat{l}_s$, the solution is computed based the equation of motion (33). For the particular case where $\hat{\mu}_0 = \hat{l}_s$, the solution is computed based on the equation of motion (46) and is shown with the symbol $\circ$ in Figs. 1 and 2. It is evident from these figures that the frequency and damping ratio solutions are continuous and do not show any sign of inconsistency.

## 6 Numerical solution of the vibration problem

The derivation of the equation of motion resulted in a linear PDE subjected to a combination of four types of boundary conditions with two applied at each boundary. Due to the complexity of the problem, a solution of the equation of motion cannot be easily obtained analytically for certain combinations of the boundary conditions. For these cases, it is preferable to rely on a numerical method such as the Differential Quadrature Method (DQM). To reduce the presence of spurious complex eigenvalues that generally occur in some DQM implementations, the equation of motion is discretized based on a Locally adaptive Differential Quadrature Method (LaDQM). LaDQM is based on the same DQM matrices, but uses external additional nodes to apply multiple boundary conditions. This ensures that all the internal nodes obey the equation of motion. This section briefly details the

implementation of the LaDQM based numerical method; Trabelssi et al. [54] give further details.

LaDQM requires the discretisation of the spatial variable, and here the mesh coordinates are given by

$$\xi_i = \begin{cases} \xi_1 - \delta\left(\xi_1 - \xi_{2-i}\right) & 1 - n_L \leq i < 1 \\ \xi_n + \delta\left(\xi_n - \xi_{2n-i}\right) & n + n_R \geq i > n \\ \dfrac{1}{2} + \dfrac{\tanh\left(\varsigma\left(\frac{i-1}{n-1} - \frac{1}{2}\right)\right)}{2\tanh\left(\frac{\varsigma}{2}\right)} & 1 \leq i \leq n \end{cases} \tag{52}$$

where $n$ is the number of internal nodes and $n_R$ and $n_L$ denote, respectively, the number of external nodes at the right and the left sides and $\varsigma$ represents a bias adjustment parameter. In the DQM approach the $m$-th derivative at the nodes is approximated by $\mathbf{M}_m\mathbf{Y}$ where $\mathbf{Y}$ is the displacement vector with $i$-th element $Y_i = \theta(\xi_i, t)$, for $1 - n_L \leq i \leq n + n_R$. The matrices, $\mathbf{M}_m$, are given by [55, 56]

$$[M_m]_{i,j} = \begin{cases} \dfrac{\Pi\xi_i}{\left(\Pi\xi_j\left[\Delta\xi\right]_{i,j}\right)} & m = 1,\ i \neq j \\ m\left\{[M_1]_{i,j}[M_{m-1}]_{i,i} - \frac{[M_{m-1}]_{i,j}}{[\Delta\xi]_{i,j}}\right\} & m > 1,\ i \neq j \\ \sum_{k=1-n_L, k\neq i}^{n+n_R}[M_m]_{i,k} & m > 0,\ i = j \end{cases} \tag{53}$$

where $[M_m]_{i,j}$ is the $(i,j)$-th element of $\mathbf{M}_m$ and

$$\begin{aligned} \left[\Delta\xi\right]_{i,j} &= \xi_i - \xi_j, \qquad 0 \leq i, j \leq n+1 \\ \Pi\xi_i &= \prod_{k=1-n_L}^{n+n_R}\left[\Delta\xi\right]_{i,k}, \qquad 0 \leq i \leq n+1 \end{aligned} \tag{54}$$

In addition, $M_0$ is defined as the identity matrix of the same order as the rest of the DQM matrices. The velocity and acceleration vectors are given by $\dot{\mathbf{Y}}$ and $\ddot{\mathbf{Y}}$.

The DQM discretization of the equation of motion, Eq. (33), is given by

$$\begin{aligned} \left[\mathbf{M}_0 - \hat{l}_k^2\mathbf{M}_2 - \hat{\mu}_0^2\left(\mathbf{M}_2 - \hat{l}_k^2\mathbf{M}_4\right)\right]\ddot{\mathbf{Y}} - \hat{g}\left[\mathbf{M}_2 - \hat{l}_s^2\mathbf{M}_4\right]\dot{\mathbf{Y}} \\ - \left[\left(\mathbf{M}_2 - \hat{l}_s^2\mathbf{M}_4\right) - \hat{k}_{EM}\left(\mathbf{M}_0 - \hat{\mu}_0^2\mathbf{M}_2\right)\right]\mathbf{Y} \;=\; 0 \end{aligned} \tag{55}$$

This equation represents a system of $n$ coupled ordinary differential equations, where the basic structure of the mass, stiffness and damping matrices are clearly defined. There are a total of $n + n_R + n_L$ equations, and a few of these will be replaced with the boundary condition equations. Four boundary equations are required for the nanorod system, and

Table 5: LaDQM mesh convergence for CF-CF case; $\hat{l}_s = \hat{l}_k = 0.4$, $\hat{\mu}_0 = 0.08$, $\hat{k}_{EM} = 1$, $\hat{g} = 0.02$.

| No. Nodes | 19 | 17 | 15 | 13 | 11 | 9 |
|---|---|---|---|---|---|---|
| $\omega_1$ | 3.1098 | 3.1098 | 3.1098 | 3.1098 | 3.1098 | 3.1094 |
| $\omega_2$ | 5.6260 | 5.6260 | 5.6260 | 5.6264 | 5.6355 | 5.8296 |
| $\omega_3$ | 7.5298 | 7.5298 | 7.5296 | 7.5280 | 7.4958 | 7.7505 |
| $\varsigma_1$ | 0.0298 | 0.0298 | 0.0298 | 0.0298 | 0.0298 | 0.0298 |
| $\varsigma_2$ | 0.0560 | 0.0560 | 0.0560 | 0.0560 | 0.0561 | 0.0581 |
| $\varsigma_3$ | 0.0752 | 0.0752 | 0.0752 | 0.0752 | 0.0749 | 0.0774 |

take the form

$$\begin{aligned} \theta|_{\xi_b} &= 0 \\ \hat{T}|_{\xi_b} &= 0 \\ - \quad &- \quad - \\ \frac{\partial \theta}{\partial \xi}|_{\xi_b} &= 0 \\ \hat{T}^{(1)}|_{\xi_b} &= 0 \end{aligned} \tag{56}$$

where $\xi_b = 1$ or 0. After rearrangement, the discrete expressions of the above boundary conditions can be written as

$$\begin{aligned} \left[\mathbf{M}_0\mathbf{Y}\right]_{n_b} &= 0 \\ \left[\hat{\mu}_0^2\left(\mathbf{M}_1 - \hat{l}_k^2\mathbf{M}_3\right)\ddot{\mathbf{Y}} + \left(\mathbf{M}_1 - \hat{l}_s^2\mathbf{M}_3\right)\left(\mathbf{Y} + \hat{g}\dot{\mathbf{Y}}\right) + \hat{\mu}_0^2\hat{k}_{EM}\mathbf{M}_1\mathbf{Y}\right]_{n_b} &= 0 \\ - \quad &- \quad - \\ \left[\mathbf{M}_1\mathbf{Y}\right]_{n_b} &= 0 \\ \left[\hat{\mu}_0^4\left(\mathbf{M}_2 - \hat{l}_k^2\mathbf{M}_4\right)\ddot{\mathbf{Y}} + \left(\left(\hat{\mu}_0^2 - \hat{l}_s^2\right)\mathbf{M}_2 - \hat{\mu}_0^2\hat{l}_s^2\mathbf{M}_4\right)\left(\hat{g}\dot{\mathbf{Y}} + \mathbf{Y}\right) + \hat{\mu}_0^4\hat{k}_{EM}\mathbf{M}_2\mathbf{Y}\right]_{n_b} &= 0 \end{aligned} \tag{57}$$

where $n_b = 0, 1, n$ or $n+1$. The boundary condition of the Dirichlet type should replace the equation of motion at the corresponding boundary node. The remaining boundary equations will replace the equation of motion at the external nodes. Once the boundary conditions have been introduced into Eq. (55) the result is a standard second order differential equation where the mass, damping and stiffness matrices are clearly identified. For the damped case the equations should be written in state space form. Standard methods to estimate the eigenvalues (natural frequency and damping ratio) and the corresponding eigenvectors (mode shapes) may be employed.

To assess the accuracy of the LaDQM results, a mesh convergence study is conducted on the nanorod in which high values of the length-scale parameters were employed and several boundary conditions were tested. Results include the first three natural frequencies and damping ratios. A sample of these results corresponding to CF-CF case are reported in Table 5 where the number of nodes is varied from 9 to 19. Based on a thorough convergence study, it is decided that a total of 15 nodes is sufficient to reach the required accuracy using the LaDQM approach.

# 7 Results and discussion

## 7.1 Validation study

The equation of motion (27) describes a damped free torsional vibration of a nanorod. A similar equation of motion was obtained by Li et al. [14] for longitudinal vibration of size-dependent rods via nonlocal strain gradient theory:

$$\left(1-\mu_0^2\frac{\partial^2}{\partial x^2}\right)\rho \mathrm{A}\frac{\partial^2 u}{\partial t^2}-\mathrm{EA}\left(1-l_s^2\frac{\partial^2}{\partial x^2}\right)\frac{\partial^2 u}{\partial x^2}=0$$

which is equivalent to Eq. (27) when setting the velocity gradient length-scale parameter $l_k$, the damping coefficient $g$ and the stiffness of the surrounding medium $k_{EM}$ to zero and noting that $\rho A \equiv \rho J$, $EA \equiv GJ$ and $u \equiv \theta$. Knowing that the non-dimensional natural frequency $\hat{\omega}=\omega L\sqrt{\frac{\rho}{G}}$, performing an analogous normalization of the natural frequencies obtained by Li et al. [14] gives

$$\omega=\frac{n\pi}{L}\sqrt{\frac{E(L^2+l_s n^2\pi^2)}{\rho(L^2+\mu_0^2 n^2\pi^2)}} \qquad \hat{\omega}=n\pi\sqrt{\frac{(1+\hat{l}_s n^2\pi^2)}{(1+\hat{\mu}_0^2 n^2\pi^2)}} \qquad CF-CF \tag{58a}$$

$$\omega=\frac{(2n-1)\pi}{2L}\sqrt{\frac{E(4L^2+l_s(2n-1)^2\pi^2)}{\rho(4L^2+\mu_0^2(2n-1)^2\pi^2)}} \quad \hat{\omega}=\frac{(2n-1)\pi}{2}\sqrt{\frac{(1+\hat{l_s}(\frac{2n-1}{2})^2\pi^2)}{(1+\hat{\mu}_0^2(\frac{2n-1}{2})^2\pi^2)}} \quad CF-FS \tag{58b}$$

which are the same the frequencies obtained in this study by solving (44) and using the appropriate expressions of $a$, $b$ and $c$ provided in Table 2. This completes the validation of the obtained results with those of Li et al. [14].

## 7.2 Comparison between analytical and numerical results

This section presents a comparison between analytical and numerical torsional vibrational non-dimensional frequencies of a size-dependent viscoelastic nanorod embedded in an elastic medium. Table 6 summarizes the considered sets of boundary conditions (CF-CF/FS-FS and CF-FS) and the values of the input parameters for the following three special cases: (i) NSG damped case where nonlocal and damping effects are accounted for; (ii) Local damped case where nonlocal effects are neglected and (iii) Local undamped case where both nonlocal and damping effects are neglected. It is worth noting that the results for both CF-CF and FS-FS boundary conditions are similar due to their identical characteristic polynomial and, therefore, the corresponding results are also similar. Non-dimensional values of the length-scale parameters, stiffness of elastic medium and damping coefficient are assumed since the literature does not provide experimental or verified simulated values. The analytically and numerically obtained eigenvalues are complex and the damping ratio and natural frequency are extracted from these eigenvalues.

It is also worth mentioning the importance of choosing the right ranges for the length-scale parameters. Ideally, the calibration of these parameters can be done either through

experiments conducted at the nano-scale which is almost impossible or through Molecular Dynamics (MD) simulations as was done by Ansari et al. [57] and this is also prohibitively computationally expensive. In the absence of experiments and MD simulations, reasonable ranges of these length-scale parameters were chosen, as indicated in Table 6. In selecting the ranges of these parameters, $\hat{\mu}_0$ and $\hat{l}_s$ are chosen such their effect will not cancel out as they have opposing effect and $\hat{l}_s$ is in the same range as $\hat{l}_k$.

Table 7 compares the analytical and numerical non-dimensional first three natural frequencies ($\omega_1$, $\omega_2$, $\omega_3$) in addition to the asymptotic natural frequency $\omega_\infty$ where the wave number $n$ goes to infinity and the corresponding damping ratios ($\zeta_1$, $\zeta_2$, $\zeta_3$, $\zeta_\infty$). It is observed that numerical solutions are in good agreement with analytical solutions up to the second decimal digit for most of the cases in the CF-CF/FS-FS boundary conditions. It is also noticed that the same trend is followed for the CF-FS boundary conditions. The asymptotic frequency estimated using LaDQM was obtained by increasing the mesh size until a frequency convergence is reached, that is when a number of higher modes all have the same frequency.

Table 6: Definition of parameters used in Table 7.

| CF-CF & FS-FS | | | | | | |
|---|---|---|---|---|---|---|
| Case | Description | $\hat{\mu}_0$ | $\hat{l}_s$ | $\hat{l}_k$ | $\hat{g}$ | $\hat{k}_{EM}$ |
| 1.1 | NSG Damped | 0.2 | 0.05 | 0.05 | 0.02 | 1 |
| 1.2 | Local Damped | 0 | 0 | 0 | 0.02 | 1 |
| 1.3 | Local Undamped | 0 | 0 | 0 | 0 | 1 |
| CF-FS | | | | | | |
| Case | Description | $\hat{\mu}_0$ | $\hat{l}_s$ | $\hat{l}_k$ | $\hat{g}$ | $\hat{k}_{EM}$ |
| 2.1 | NSG Damped | 0.2 | 0.05 | 0.05 | 0.02 | 1 |
| 2.2 | Local Damped | 0 | 0 | 0 | 0.02 | 1 |
| 2.3 | Local Undamped | 0 | 0 | 0 | 0 | 1 |

### 7.3 Parametric study

This section presents results of the non-dimensional natural frequencies and damping ratios of the size-dependent viscoelastic torsional nanorod embedded in an elastic medium. In this parametric study, it was verified that numerical and analytical results show good agreement for all three cases of boundary conditions and therefore analytical results will be used in all figures except otherwise mentioned. The primary objective of this study is to investigate the effect of the length-scale parameters, namely, nonlocal, strain gradient and velocity gradient parameters denoted, respectively, $\hat{\mu}_0$, $\hat{l}_s$ and $\hat{l}_k$. In addition, the effect of viscoelastic parameters $\hat{g}$, stiffness coefficient of elastic medium $\hat{k}_{EM}$ and different boundary conditions is also examined. After several iterations, it was decided to consider the following values of the input parameters: $\hat{\mu}_0 = 0, 0.08$, $\hat{g} = 0.01, 0.015, 0.02$, $\hat{k}_{EM} = 0, 2$ while $\hat{l}_s$ and $\hat{l}_k$ were varied in the interval $[0.1, 0.4]$.

Table 7: Comparison between analytical and numerical solutions.

| | | Analytical | | | | LaDQM | | | |
|---|---|---|---|---|---|---|---|---|---|
| | | n | | | | n | | | |
| Cases | | 1 | 2 | 3 | $\infty$ | 1 | 2 | 3 | $\infty$ |
| 1.1 | $\omega$ | 2.8376 | 4.0270 | 4.5086 | 5.0000 | 2.8336 | 4.0148 | 4.4929 | 4.9975 |
| | $\varsigma$ | 0.0250 | 0.0380 | 0.0433 | 0.0500 | 0.0249 | 0.0378 | 0.0430 | 0.0499 |
| 1.2 | $\omega$ | 3.2969 | 6.3623 | 9.4777 | | 3.2968 | 6.3601 | 9.4857 | |
| | $\varsigma$ | 0.0299 | 0.0621 | 0.0937 | | 0.0299 | 0.0620 | 0.0938 | |
| 1.3 | $\omega$ | 3.2969 | 6.3623 | 9.4777 | | 3.2968 | 6.3602 | 9.4857 | |
| | $\varsigma$ | 0.0000 | 0.0000 | 0.0000 | | 0.0000 | 0.0000 | 0.0000 | |
| 2.1 | $\omega$ | 1.7999 | 3.5648 | 4.3193 | 5.0000 | 1.8577 | 3.6432 | 4.3632 | 4.9948 |
| | $\varsigma$ | 0.0125 | 0.0330 | 0.0412 | 0.0500 | 0.0132 | 0.0339 | 0.0417 | 0.0493 |
| 2.2 | $\omega$ | 1.8621 | 4.8173 | 7.9174 | | 1.8690 | 4.8387 | 7.8946 | |
| | $\varsigma$ | 0.0133 | 0.0461 | 0.0779 | | 0.0133 | 0.0463 | 0.0777 | |
| 2.3 | $\omega$ | 1.8621 | 4.8173 | 7.9174 | | 1.8690 | 4.8387 | 7.8946 | |
| | $\varsigma$ | 0.0000 | 0.0000 | 0.0000 | | 0.0000 | 0.0000 | 0.0000 | |

### 7.3.1 CF-CF and FS-FS Cases

The analytical results for both CF-CF and FS-FS boundary conditions are similar due to their identical characteristic polynomial. Figure 3 shows the variation of the non-dimensional first mode frequency and damping ratio for increasing values of $\hat{l}_s$ and fixed values of $\hat{\mu}_0$, $\hat{l}_k$, $\hat{k}_{EM}$ and $\hat{g}$. The upper four plots indicate an almost linearly increasing trend of the first mode frequency for increasing values of $\hat{l}_s$. The trend for the damping ratio is also similar and varies linearly, as evident from the lower four plots. It can also be observed that the first mode frequency and damping ratio decrease as the kinetic length scale parameter $\hat{l}_k$ increases for fixed $\hat{l}_s$. In addition, increasing the viscoelastic coefficient $\hat{g}$ seems to have no effect on the natural frequency but increases linearly the damping ratio. Furthermore, accounting for the medium stiffness $\hat{k}_{EM}$ increases slightly the frequency however slightly decreases the damping ratio. Moreover, increasing $\hat{\mu}_0$ has a tendency to decrease the frequency and to a lesser extent the damping ratio. The opposite effect is observed when increasing $\hat{l}_s$ as mentioned above.

Figures 4 and 5 illustrate, respectively, the effect of the variation of the non-dimensional second and third mode frequencies and damping ratios for increasing values of $\hat{l}_s$ and fixed values of $\hat{\mu}_0$, $\hat{l}_k$, $\hat{k}_{EM}$ and $\hat{g}$. Similar observations can be made as the first mode of vibration. However, the frequencies and damping ratios curves shift to higher values for the second and third modes.

### 7.3.2 CF-FS Case

The analytical results of the torsional vibrational size-dependent viscoelastic nanorod for CF-FS boundary conditions are presented now. Figures 6, 7 and 8 illustrate, respectively, the effect of the variation of the non-dimensional first, second and third mode frequencies and damping ratios for increasing values of $\hat{l}_s$ and fixed values of $\hat{\mu}_0$, $\hat{l}_k$, $\hat{k}_{EM}$ and $\hat{g}$. The same remarks made about the CF-CF boundary condition are also valid in this case apart from a few exceptions. From Figure 6, it can be observed that the variation of frequencies

and damping ratios curves seem to be small and of about the same amount as compared to the CF-CF boundary condition. The effect of damping ratios curves decrease as the $\hat{l}_k$ value increases and the remaining predictions are the same as the first mode with the CF-CF boundary condition. Moreover, the first mode frequency increases significantly and decreases the damping ratio drastically when accounting for the stiffness medium $\hat{k}_{EM}$.

Figure 7 and 8 show similar trends as the second and third modes with the CF-CF boundary condition. It is also clear that the variation of the frequency curves appears to be large for increasing values of $\hat{l}_k$ whereas the variation of the damping ratio curves seems to be substantial and decreases as the $\hat{l}_k$ value increases for the second and third modes of vibration.

### 7.3.3 CS-CS Case

The Clamped Strained-Clamped Strained (CS-CS) configuration is one of the cases where an analytical expression of the mode shapes is difficult to obtain. Thus the results were computed numerically using LaDQM. Based on Eqs. (34a) and (34b), the boundary conditions for this case are $\theta = 0$ and $\frac{\partial \theta}{\partial \xi} = 0$ specified at each of the ends $\xi = 0$ and $\xi = 1$.

The results are plotted in Figures 9, 10 and 11 and are similar to the previous cases. Compared to the CF-CF case the CS-CS case plots show similar trends for both frequencies and damping ratios especially the hardening and softening effect associated with the different material length scales. However, compared to the CF-CF case, the results show a rise in all natural frequencies and damping ratios. It is also observed that the impact of foundation stiffness is severely reduced even for the first mode. Compared to the CF-CF case, the first mode frequency displays a linear like dependency on $\hat{l}_s$ and a higher non-linear dependency on $\hat{l}_k$. Such behavior was observed for higher modes in the CF-CF case.

A shift to higher mode behavior is also observed in the damping ratios plots. The first mode damping ratios show a severe dependence on $\hat{l}_k$ and $\hat{l}_s$. However, unlike $\hat{k}_{EM}$, the influence of the damping coefficient $\hat{g}$ is still visible in the first three modes.

## 8 Conclusion

A combined nonlocal strain and velocity gradient theory was used to study the size-dependent torsional vibration of a viscoelastic nanorod embedded in an elastic medium. Three material length-scale parameters were incorporated in the model namely nonlocal, strain gradient and velocity gradient parameters with the capability of modeling both softening and hardening behavior. The Kelvin–Voigt viscoelastic damping was integrated to account for the viscoelastic behavior which added a damping term to the constitutive equation. The equation of motion and the related boundary conditions were derived using the Hamiltonian principle. The linear free vibration of the nanorod embedded in an elastic medium was investigated with a combination of clamped forcing and free strained boundary conditions. Frequencies and damping ratios were obtained both analytically and numerically using a Locally adaptive Differential Quadrature Method (LaDQM). Analytical results were obtained for various length-scales and compared with LaDQM numerical results.

The parametric study investigated the effect of the length-scale and viscoelastic parameters, medium's stiffness and different boundary conditions. The main conclusions can be summarized as follows: (a) the strain gradient and nonlocal parameters $l_s$ and $\mu_0$ seem to have opposite effects resulting, respectively, in a hardening and softening behavior; (b) the effect of the medium's stiffness $k_{EM}$ is small and limited mainly to the first mode but its

effect might increase if a larger value was used; (c) the effect of the damping coefficient $g$ is limited to the damping ratios and significantly affected by $l_k$ and $\mu_0$ especially for high modes and (d) the effect of the velocity gradient parameter $l_k$ resulted in a space dependent and thus a mode dependent effective mass, thereby, causing a decrease of the frequencies particularly for high modes.

The case where the strain gradient and nonlocal parameters are equal ($l_s = \mu_0$) may seem to result in an inconsistency to the general equation of motion and the related non-classical boundary conditions. A study of this case was treated thoroughly in this paper demonstrating that the proposed solution would not show any inconsistency.

**Acknowledgements.** The first author acknowledges the financial support of Texas A&M University at Qatar. The last author is grateful to the Oscar S. Wyatt Endowed Chair.

## References


[1] A.C. Eringen, D.G.B. Edelen, On nonlocal elasticity, International Journal of Engineering Science, 10 (1972), 233-248.

[2] A.C. Eringen, On differential equations of non local elasticity and solutions of screw dislocation and surface waves, Journal of Applied Physics, 54 (1983), 4703-4710.

[3] A.C.Eringen, Nonlocal Continuum Field Theories,Springer-Verlag, NewYork, USA, 2002.

[4] X. Zhu, L. Li, Closed form solution for a nonlocal strain gradient rod in tension, International Journal of Engineering Science, 119 (2017) 16-28.

[5] M.A. Eltaher, S.El-Borgi, J.N. Reddy, Nonlinear Analysis of Size-dependent and Material-Dependent Nonlocal CNTs. Composite Structures, 153 (2016) 902-913.

[6] M.A. Eltaher, M.A. Agwa, Analysis of size-dependent mechanical properties of CNTs mass sensor using energy equivalent model. Sensors and Actuators A: Physical, 246 (2016) 9-17.

[7] M.A. Eltaher, S.A. Emam, F.F. Mahmoud, Free vibration analysis of functionally graded size-dependent nanobeams. Applied Mathematics and Computation, 218-14 (2012) 7406-7420.

[8] M.A. Eltaher, M.E. Khater, S.A. Emam, A review on nonlocal elastic models for bending, buckling, vibrations, and wave propagation of nanoscale beams. Applied Mathematical Modelling, 40-5 (2016) 4109-4128.

[9] R.D. Mindlin, Micro-structure in Linear Elasticity, Archive for Rational Mechanics and Analysis, 16 (1964) 51-78.

[10] E.C. Aifantis, On the role of gradients in the localization of deformation and fracture, International Journal of Engineering Science, 30 (1992) 1279-1299.

[11] F. Yang, A. Chong, D.C. Lam, P. Tong, Couple stress based strain gradient theory for elasticity, International Journal of Solids and Structures, 39 (2002), 2731-2743.

[12] Y. Tian, B. Xu, D. Yu, Y. Ma, Y. Wang, Y. Jiang, Ultrahard nanotwinned cubic boron nitride. Nature, 493 (2013), 385-388.

[13] C.W. Lim, G. Zhang, J.N. Reddy, A higher-order nonlocal elasticity and strain gradient theory and its applications in wave propagation. Journal of the Mechanics and Physics of Solids, 78 (2015), 298-313.

[14] L. Li, Y. Hu, X. Li, Longitudinal vibration of size-dependent rods via nonlocal strain gradient theory, International Journal of Mechanical Sciences, 115-116 (2016) 135-144.

[15] S. Guo, Y. He, D. Liu, J. Lei, L. Shen, Z. Li, Torsional vibration of carbon nanotube with axial velocity and velocity gradient effect, International Journal of Mechanical Sciences, 119 (2016), 88-96.

[16] Y. Shen, Y. Chen, L. Li, Torsion of a functionally graded material, International Journal of Engineering Science, 109 (2016) 14-28.

[17] R. Fernandes, S. El-Borgi, S.M. Mousavi, J.N. Reddy, A. Mechmoum, Nonlinear size-dependent longitudinal vibration of carbon nanotubes embedded in an elastic medium, Physica E, 88 (2017) 18-25.

[18] L. Li, Y. Hu, L. Ling, Flexural wave propagation in small-scaled functionally graded beams via a nonlocal strain gradient theory, Composite Structures, 133 (2015) 1079-1092.

[19] M. Simsek, Nonlinear free vibration of a functionally graded nanobeam using nonlocal strain gradient theory and a novel hamiltonian approach, International Journal of Engineering Science, 105 (2016) 12-27.

[20] L. Li, Y. Hu, Nonlinear bending and free vibration analyses of nonlocal strain gradient beams made of functionally graded material, International Journal of Engineering Science, 107 (2016a), 77-97.

[21] L. Li, Y. Hu, Wave propagation in fluid-conveying viscoelastic carbon nanotubes based on nonlocal strain gradient theory, Computational Materials Science, 112 (2016b) 282-288.

[22] L. Li, Y. Hu, Post-buckling analysis of functionally graded nanobeams incorporating nonlocal stress and microstructure-dependent strain gradient effects, International Journal of Mechanical Sciences, 120 (2017) 159-170.

[23] X. Li, L. Li, Y. Hu, Z. Ding, W. Deng, Bending,buckling and vibration of axially functionally graded beams based on nonlocal strain gradient theory, Composite Structures, 165 (2017) 250-265.

[24] M.R. Barati, A. Zenkour, A general bi-helmholtz nonlocal strain-gradient elasticity for wave propagation in nanoporous graded double-nanobeam systems on elastic substrate, Composite Structures, 168 (2017) 885-892.

[25] F. Ebrahimi, M.R. Barati, A. Dabbagh, A nonlocal strain gradient theory for wave propagation analysis in temperature-dependent inhomogeneous nanoplates, International Journal of Engineering Science, 107 (2016) 169-182.

[26] F. Ebrahimi, A. Dabbagh, Nonlocal strain gradient based wave dispersion behavior of smart rotating magneto-electro-elastic nanoplates, Materials Research Express, 4 (2016) 025003.

[27] F. Ebrahimi, A. Dabbagh, On flexural wave propagation responses of smart fg magneto-electro-elastic nanoplates via nonlocal strain gradient theory, Composite Structures, 162 (2017b) 281-293.

[28] S.J. Papadakis, A.R. Hall, P.A. Williams, L. Vicci, M.R. Falvo, R. Superfine, S. Washburn, Exact variational nonlocal stress modeling with asymptotic higher-order strain gradients for nanobeams, Physical Review Letters, 93-14 (2004), 146101.

[29] T. Fujita, K. Maenaka, Y. Takayama, Dual-axis MEMS mirror for large deflection-angle using SU-8 soft torsion beam, Sensors and Actuators A, 121 (2005), 16-21.

[30] J.M. Huang, A.Q. Liu, Z.L. Deng, Q.X. Zhang, A modeling and analysis of spring-shaped torsion micromirrors for low-voltage applications, International Journal of Mechanical Sciences, 48 (2006), 650-661.

[31] A. Arslan, D. Brown, W. Davis, S. Holmstrom, S.K. Gokce, H. Urey, Comb-actuated resonant torsional microscanner with mechanical amplification, Journal of Microelectromechanical Systems, 19 (2010), 936-943.

[32] C.W. Lim, C. Li, J.L. Yu, Free torsional vibration of nanotubes based on nonlocal stress theory, Journal of Sound and Vibration, 331 (2012) 2798-2808.

[33] C.W. Lim, M.Z. Islam, G. Zhang, A nonlocal finite element method for torsional statics and dynamics of circular nano structures, International Journal of Mechanical Sciences, 94-95 (2015) 232-243.

[34] C. Demir, O. Civalek, Torsional and longitudinal frequency and wave response of microtubules based on the nonlocal continuum and nonlocal discrete models, Applied Mathematical Modelling, 37 (2013) 9355-9367.

[35] M. Arda, M. Aydogdu, Torsional statics and dynamics of nanotubes embedded in an elastic medium, Composite Structures, 114 (2014) 80-91.

[36] Z. Islam, P. Jia, C. Lim, Torsional wave propagation and vibration of circular nanostructures based on nonlocal elasticity theory, International Journal of Applied Mechanics, 6 (2014) 1450011.

[37] C. Li, Torsional vibration of carbon nanotubes: Comparison of two nonlocal models and a semi-continuum model, International Journal of Mechanical Sciences, 82 (2014) 25-31.

[38] L. Li, Y. Hu, Torsional vibration of bi-directional functionally graded nanotubes based on nonlocal elasticity theory, Composite Structures, 172 (2017) 242-250.

[39] M.H. Kahrobaiyan, S.A. Tajalli, M.R. Movahhedy, J. Akbari, M.T. Ahmadian, Torsion of strain gradient bars, Inter. Journal of Eng. Science, 49 (2011) 856-866.

[40] A.E. Assie, M.A. Eltaher, F.F. Mahmoud, Modeling of viscoelastic contact-impact problems, Applied Mathematical Modelling, 34 (2010) 2336-2352.

[41] A.E. Assie, M.A. Eltaher, F.F. Mahmoud, The response of viscoelastic-frictionless bodies under normal impact, International Journal of Mechanical Sciences, 52 (2010) 446-454.

[42] Y. Lei, S. Adhikari, M.I. Friswell, Vibration of nonlocal Kelvin–Voigt viscoelastic damped Timoshenko beams, International Journal of Engineering Science, 66-67 (2013) 1-13.

[43] D. Karlicic, M. Cajic, T. Murmu, S. Adhikari, Nonlocal longitudinal vibration of viscoelastic coupled double-nanorod systems, European Journal of Mechanics A/Solids, 49 (2015) 183-196.

[44] D. Polyzos, G. Huber, G. Mylonakis, T. Triantafyllidis, S. Papargyri-Beskou, D.E. Beskos, Torsional vibrations of a column of fine-grained material: A gradient elastic approach, Journal of the Mechanics and Physics of Solids, 76 (2015) 338-358.

[45] F. Ebrahimi, M.R. Barati, Hygrothermal effects on vibration characteristics of viscoelastic FG nanobeams based on nonlocal strain gradient theory, Composite Structures, 159 (2017) 433-444.

[46] Y. Zare, Modeling of tensile modulus in polymer/carbon nanotubes (CNT) nanocomposites, Synthetic Metals 202 (2015) 68-72.

[47] J.C. Kearns and R.L. Shambaugh, Polypropylene fibers reinforced with carbon nanotubes, Journal of Applied Polymer Science 86 (2002) 2079-2084.

[48] M. Cadek, J.N. Coleman, V. Barron, K. Hedicke and W.J. Blau, Morphological and mechanical properties of carbon-nanotube-reinforced semicrystalline and amorphous polymer composites, Applied Physics Letters 81 (2002) 5123-5125.

[49] T.D. Fornes, J.W. Baur, Y. Sabba and E.L. Thomas, Morphology and properties of melt-spun polycarbonate fibers containing single- and multi-wall carbon nanotubes, Polymer 47 (2006) 1704-1714.

[50] M. Aydogdu, Axial vibration analysis of nanorods (carbon nanotubes) embedded in an elastic medium using nonlocal elasticity, Mech. Res. Com., 43 (2012) 34-40.

[51] T. Murmu, S.C. Pradhan, Thermo-mechanical vibration of a single-walled carbon nanotube embedded in an elastic medium based on nonlocal elasticity theory, Computational Materials Science, 46 (2009) 854-859.

[52] X.-J Xu, B. Zhou, M.-L. Zheng, Comment on "Free vibration analysis of nonlocal strain gradient beams made of functionally graded material", International Journal of Engineering Science, 119 (2017) 189-191.

[53] Y. Lei, S. Adhikari, T. Murmu, M.I. Friswell, Asymptotic frequencies of various damped nonlocal beams and plates, Mechanics Research Communications, 62 (2014) 94-101.

[54] M. Trabelssi, S. El-Borgi, L.-L. Ke, J.N. Reddy, Nonlocal free vibration of graded nanobeams resting on a nonlinear elastic foundation using DQM and LaDQM, Composite Structures,176 (2017), 736-747.

[55] C. Shu, Differential quadrature and its application in engineering, Springer, London

(2000).
[56] Z. Zong, Y. Zhang, Advanced differential quadrature methods, CRC Press (2009).
[57] R. Ansari, H. Rouhi, S. Sahmani, Calibration of the analytical nonlocal shell model for vibrations of double-walled carbon nanotubes with arbitrary boundary conditions using molecular dynamics, International Journal of Mechanical Sciences, 53 (2011) 786-792.

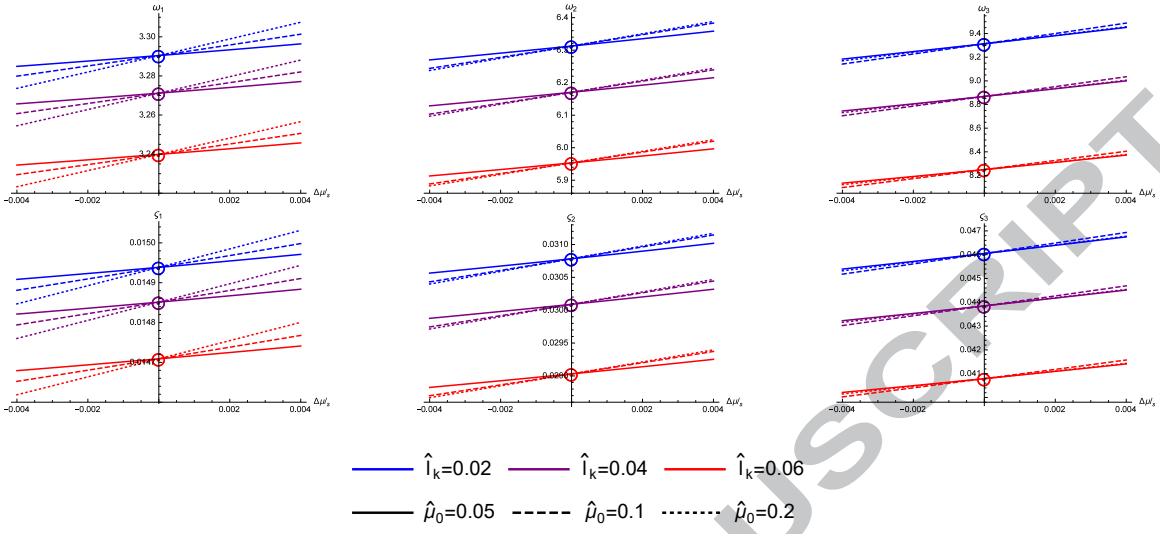


Fig. 1: Variation of the first three frequencies and damping ratios as a function of $\Delta\mu l_s = \hat{l}_s - \hat{\mu}_0$ for CF-CF / FS-FS boundary conditions (ie, when $\hat{\mu}_0$ is equal or close to $\hat{l}_s$); $\hat{k}_{EM} = 1$; Symbol $\circ$ in the plot is obtained from solution of particular case $\hat{\mu}_0 = \hat{l}_s$ given in Table 2.

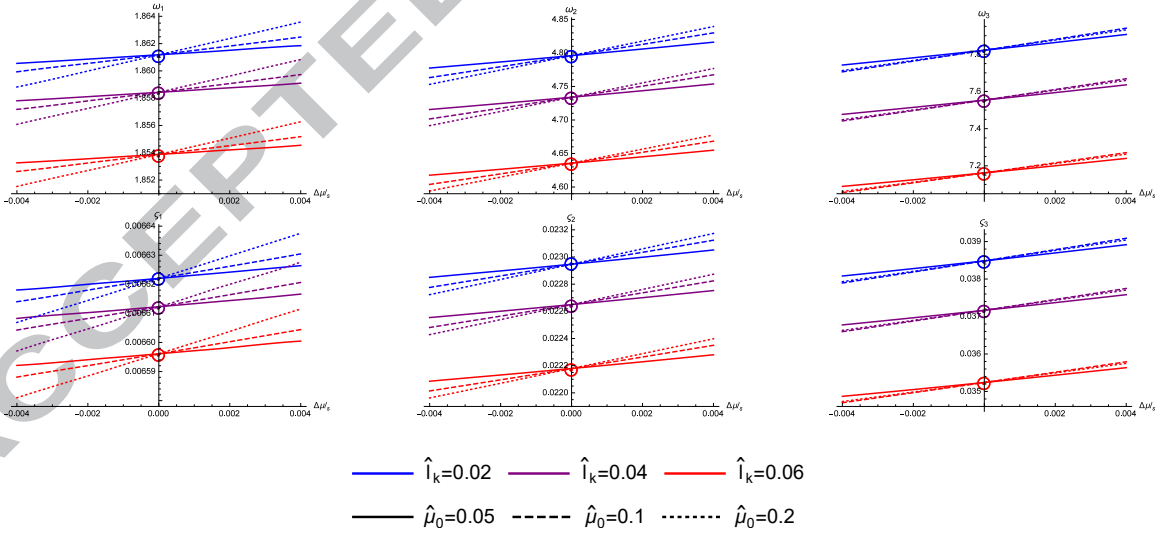


Fig. 2: Variation of the first three frequencies and damping ratios as a function of $\Delta\mu l_s = \hat{l}_s - \hat{\mu}_0$ for CF-FS boundary conditions (ie, when $\hat{\mu}_0$ is equal or close to $\hat{l}_s$); $\hat{k}_{EM} = 1$; Symbol $\circ$ in the plot is obtained from solution of particular case $\hat{\mu}_0 = \hat{l}_s$ given in Table 2.

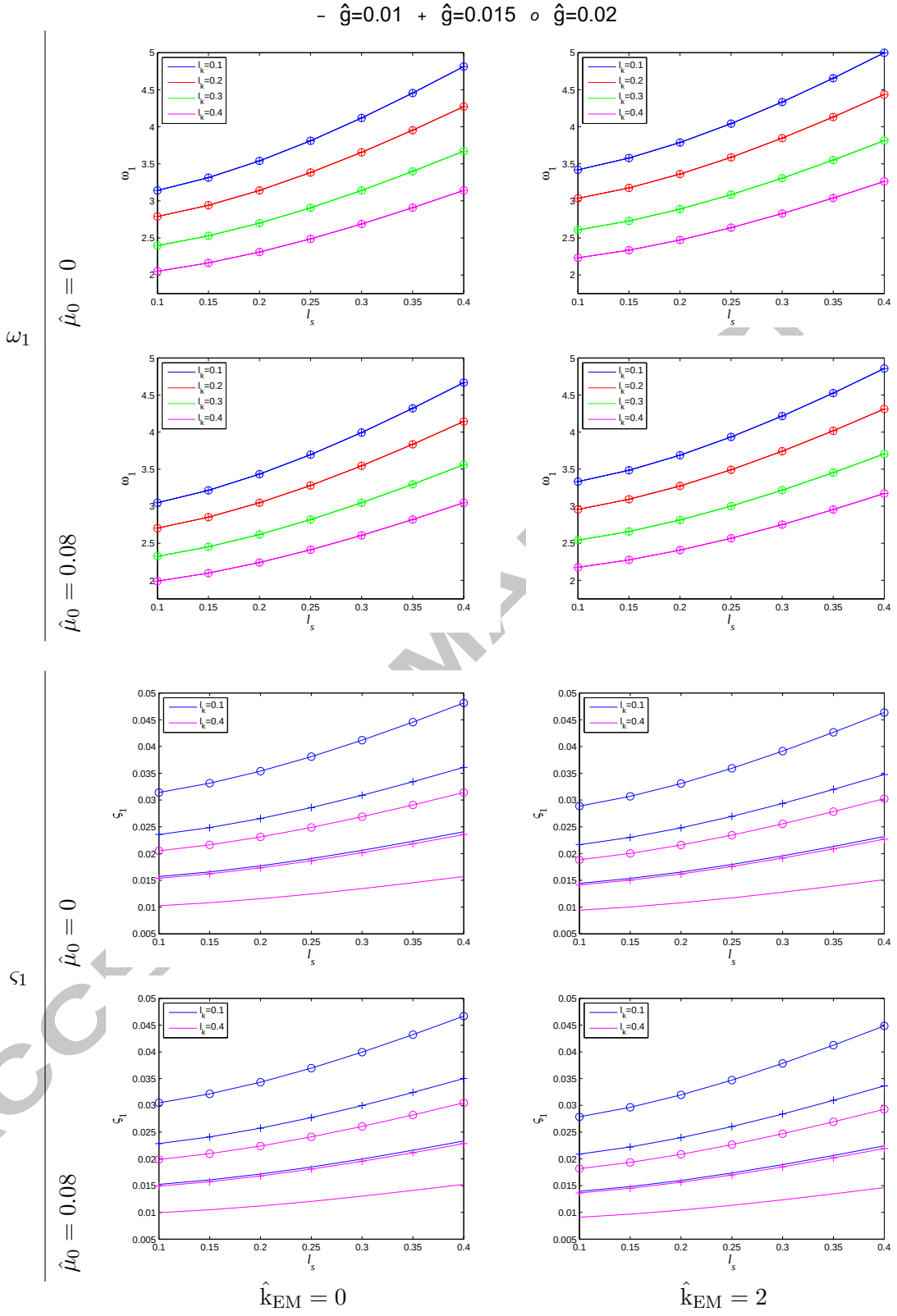


Fig. 3: Effect of length-scale parameters, stiffness of surrounding medium, and damping coefficient on the first mode frequency and damping ratio for CF-CF and FS-FS boundary conditions.

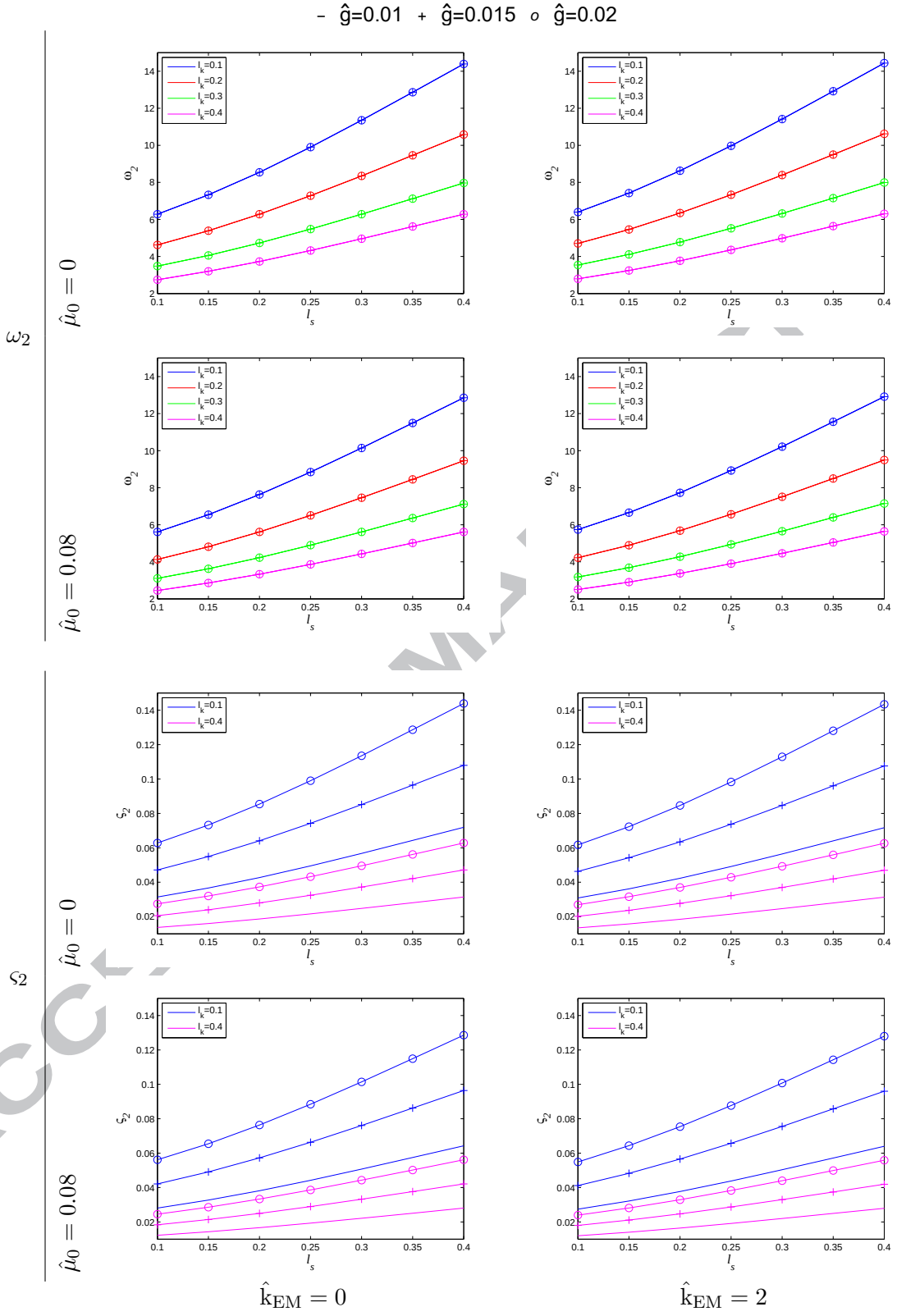


Fig. 4: Effect of length-scale parameters, stiffness of surrounding medium, and damping coefficient on the second mode frequency and damping ratio for CF-CF and FS-FS boundary conditions.

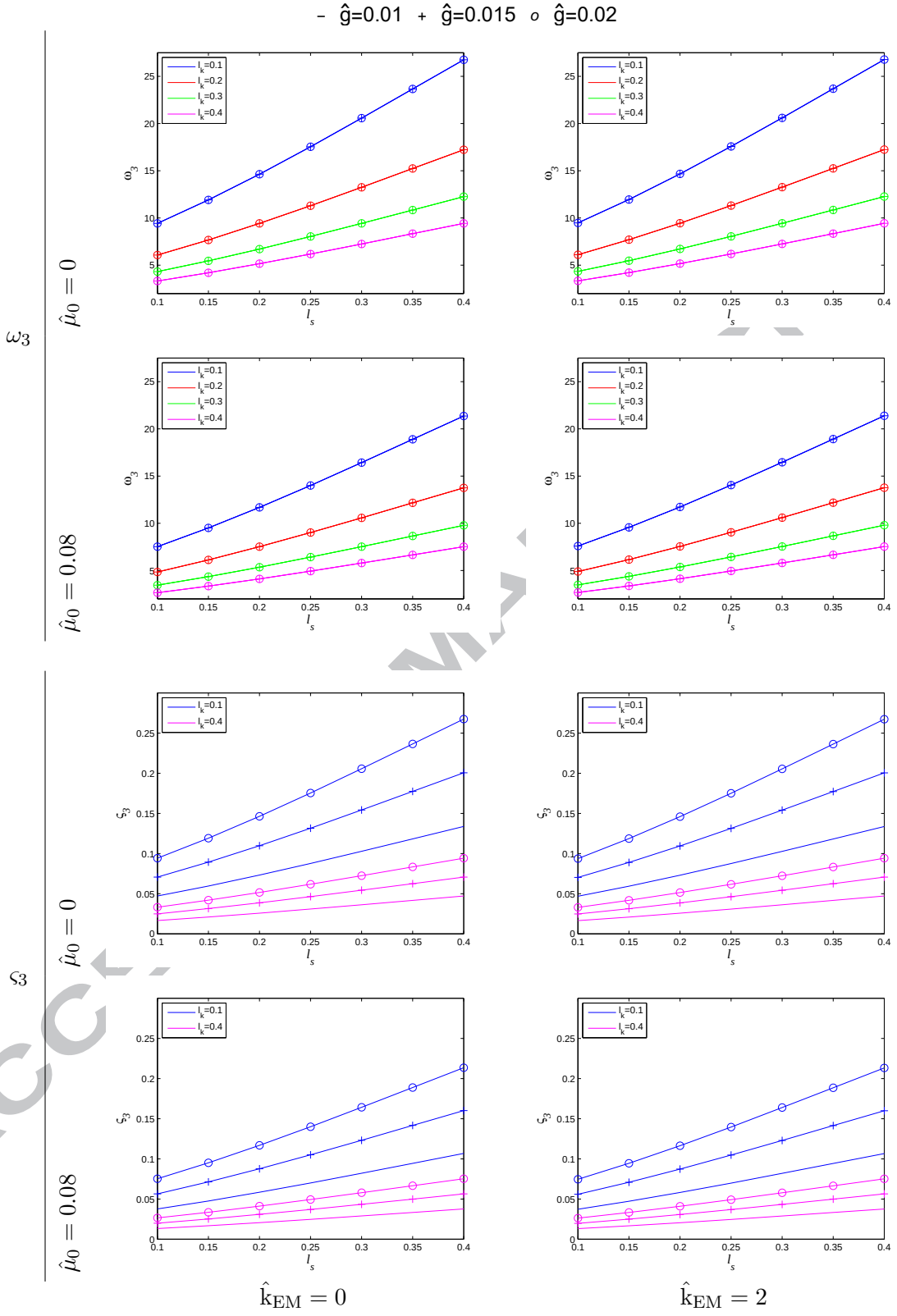


Fig. 5: Effect of length-scale parameters, stiffness of surrounding medium, and damping coefficient on the third mode frequency and damping ratio for CF-CF and FS-FS boundary conditions.

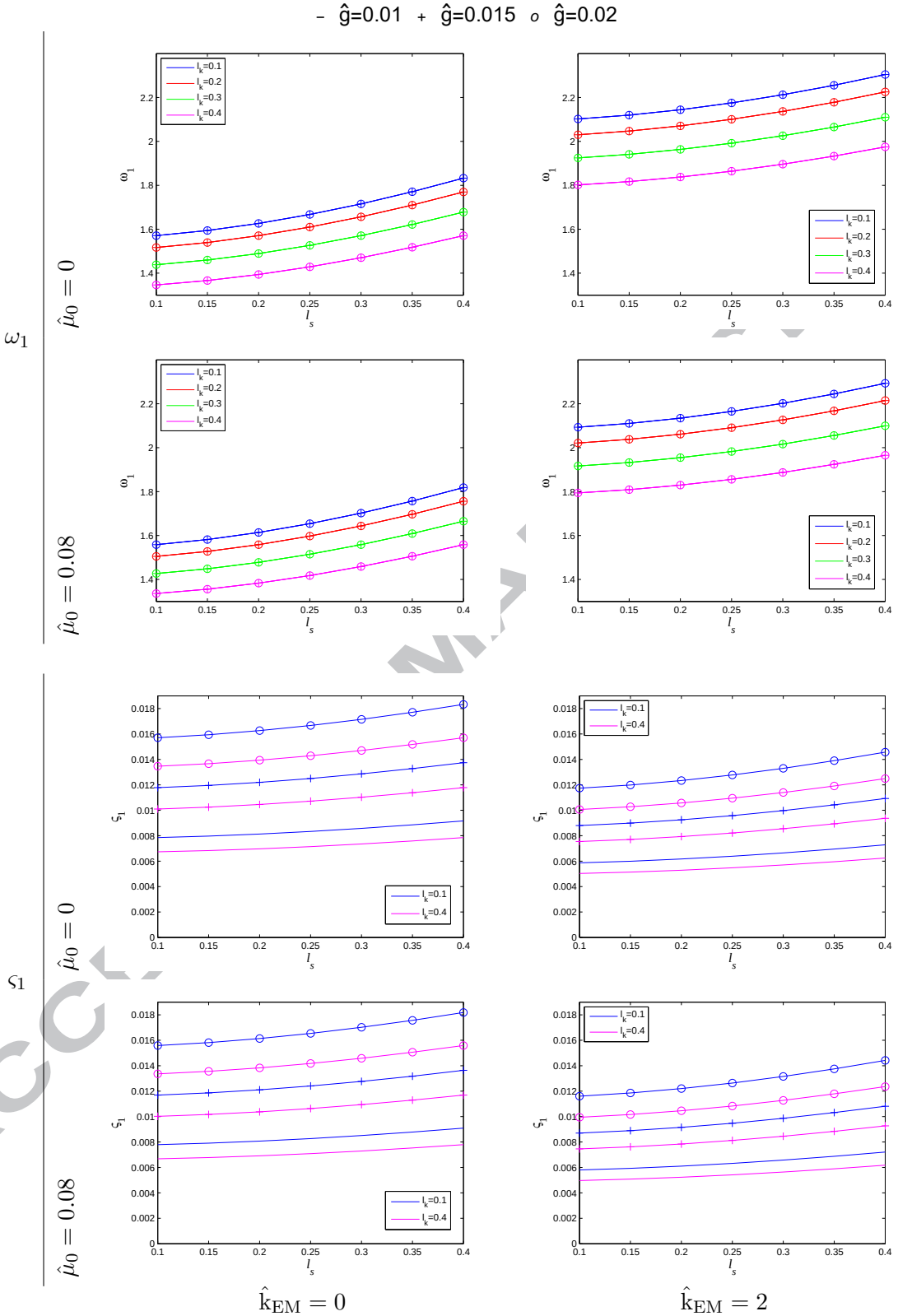


Fig. 6: Effect of length-scale parameters, stiffness of surrounding medium, and damping coefficient on the first mode frequency and damping ratio for CF-FS boundary conditions.

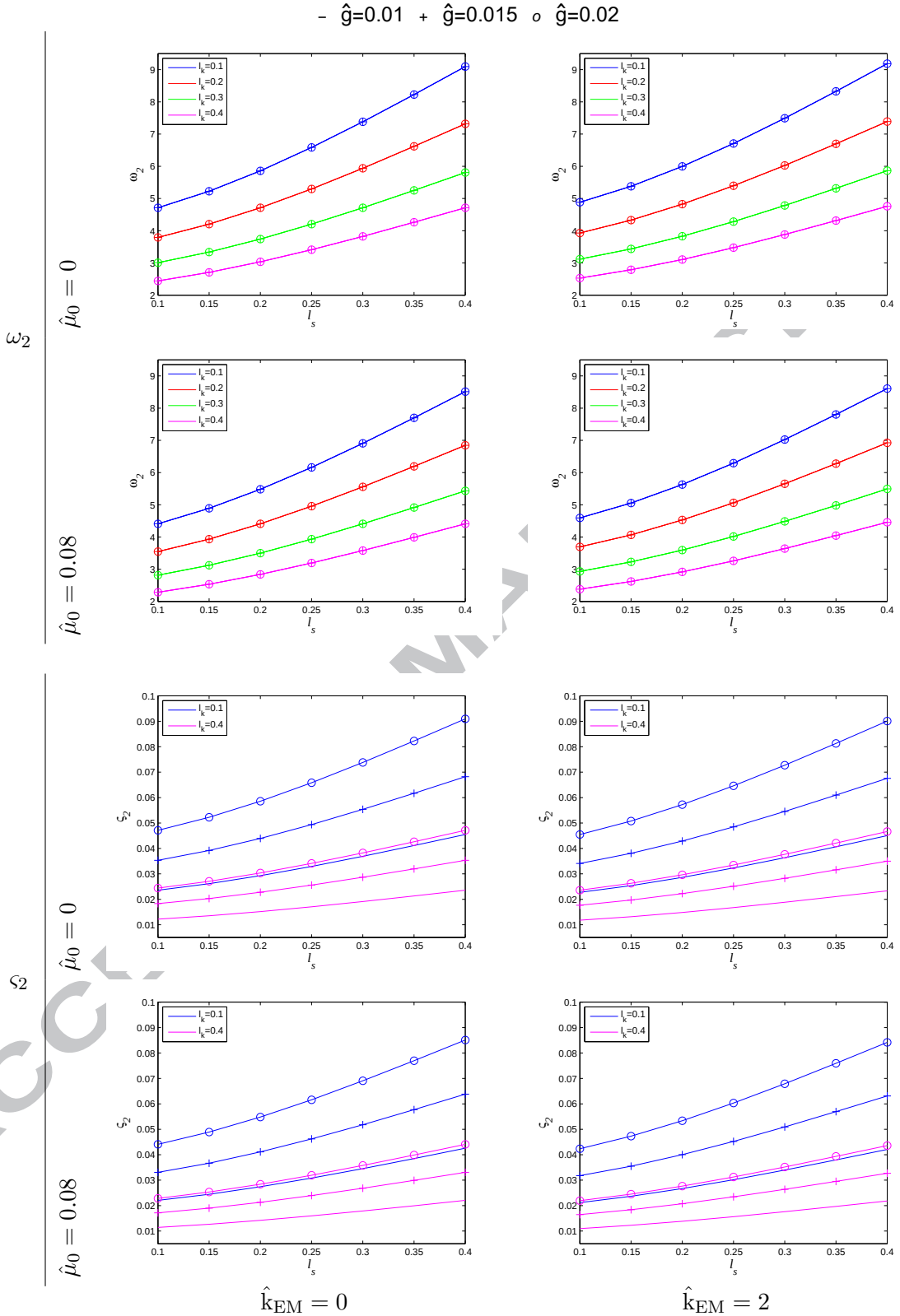


Fig. 7: Effect of length-scale parameters, stiffness of surrounding medium, and damping coefficient on the second mode frequency and damping ratio for CF-FS boundary conditions.

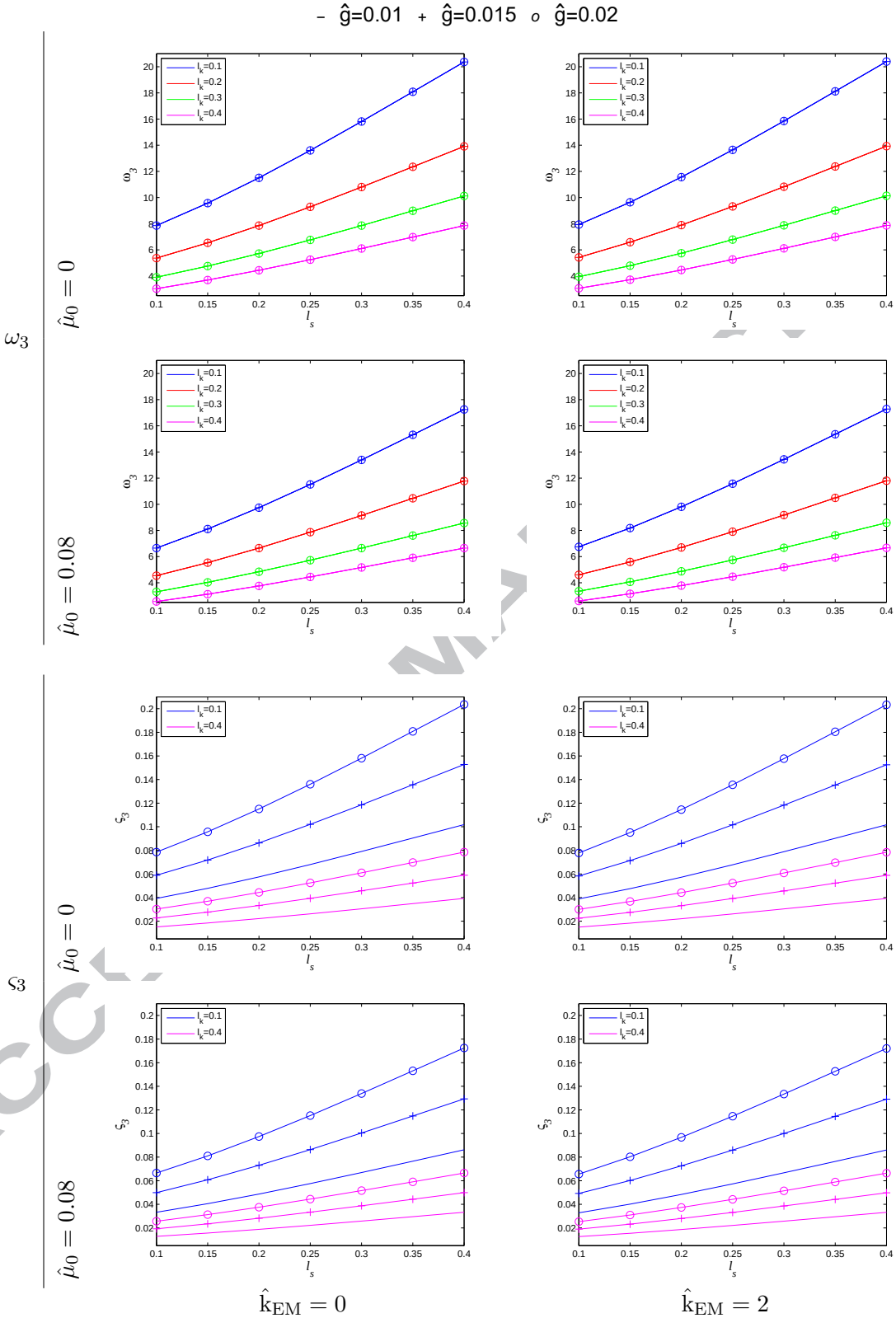


Fig. 8: Effect of length-scale parameters, stiffness of surrounding medium, and damping coefficient on the third mode frequency and damping ratio for CF-FS boundary conditions.

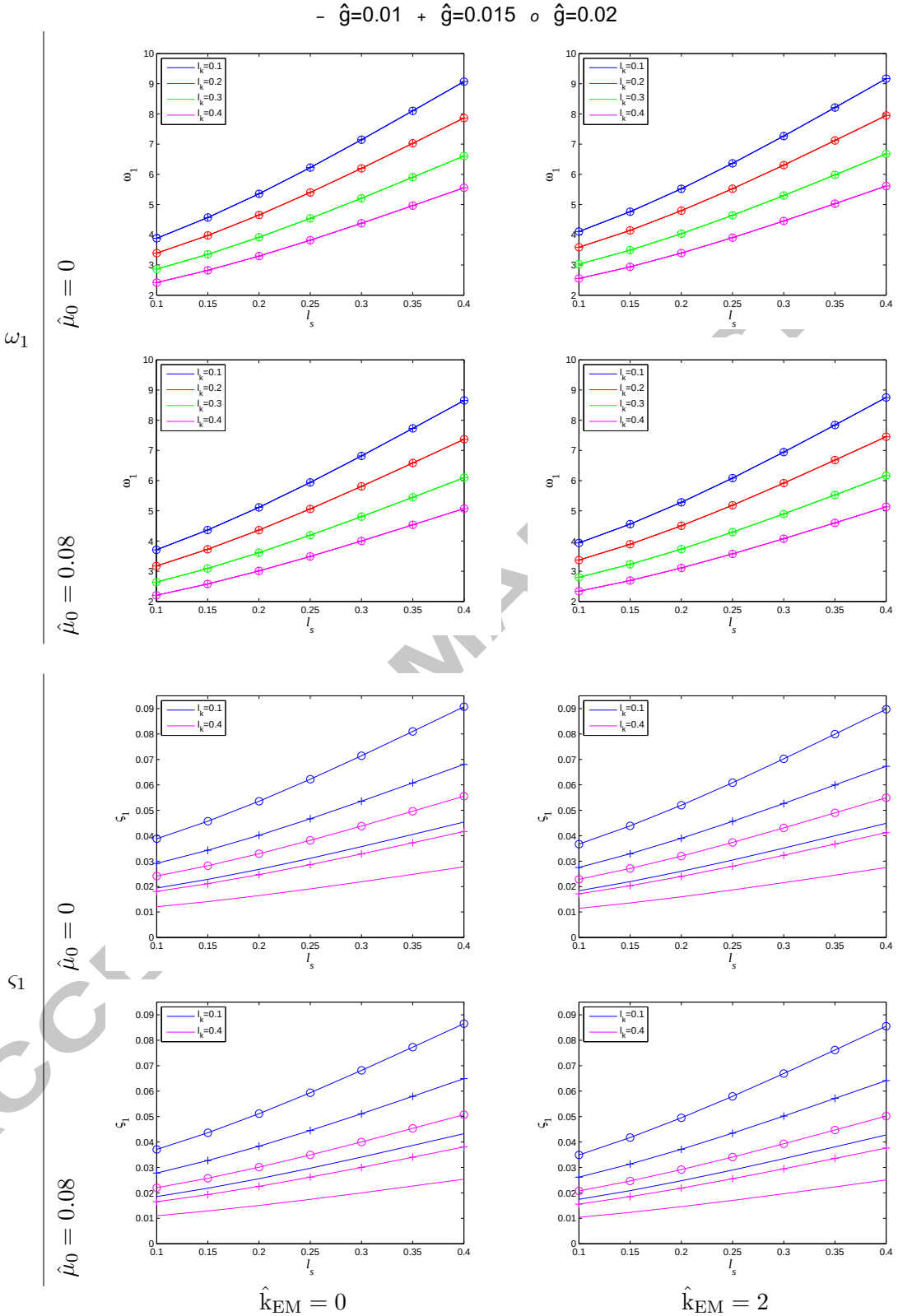


Fig. 9: Effect of length-scale parameters, stiffness of surrounding medium, and damping coefficient on the first mode frequency and damping ratio for CS-CS boundary conditions.

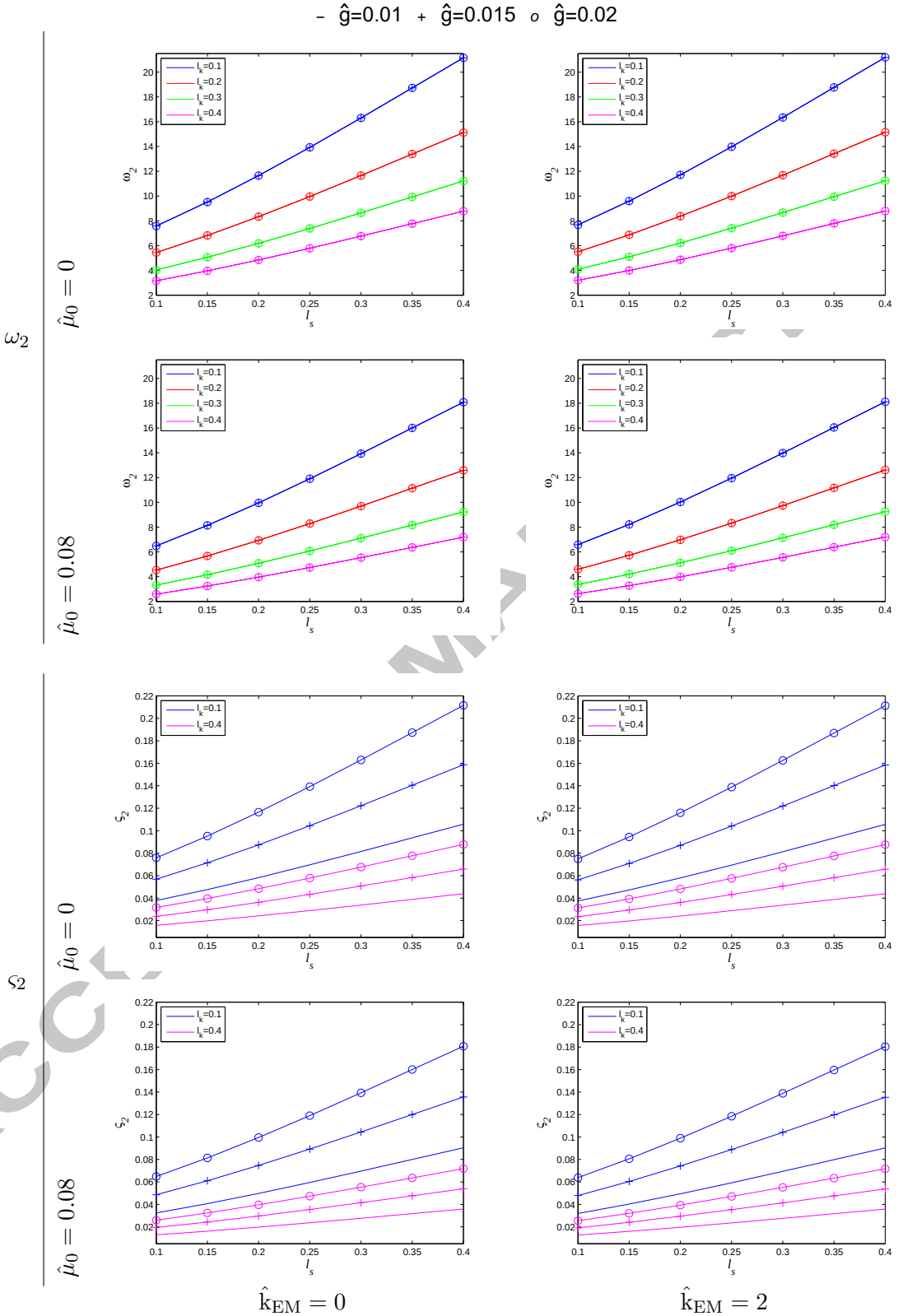


Fig. 10: Effect of length-scale parameters, stiffness of surrounding medium, and damping coefficient on the second mode frequency and damping ratio for CS-CS boundary conditions.

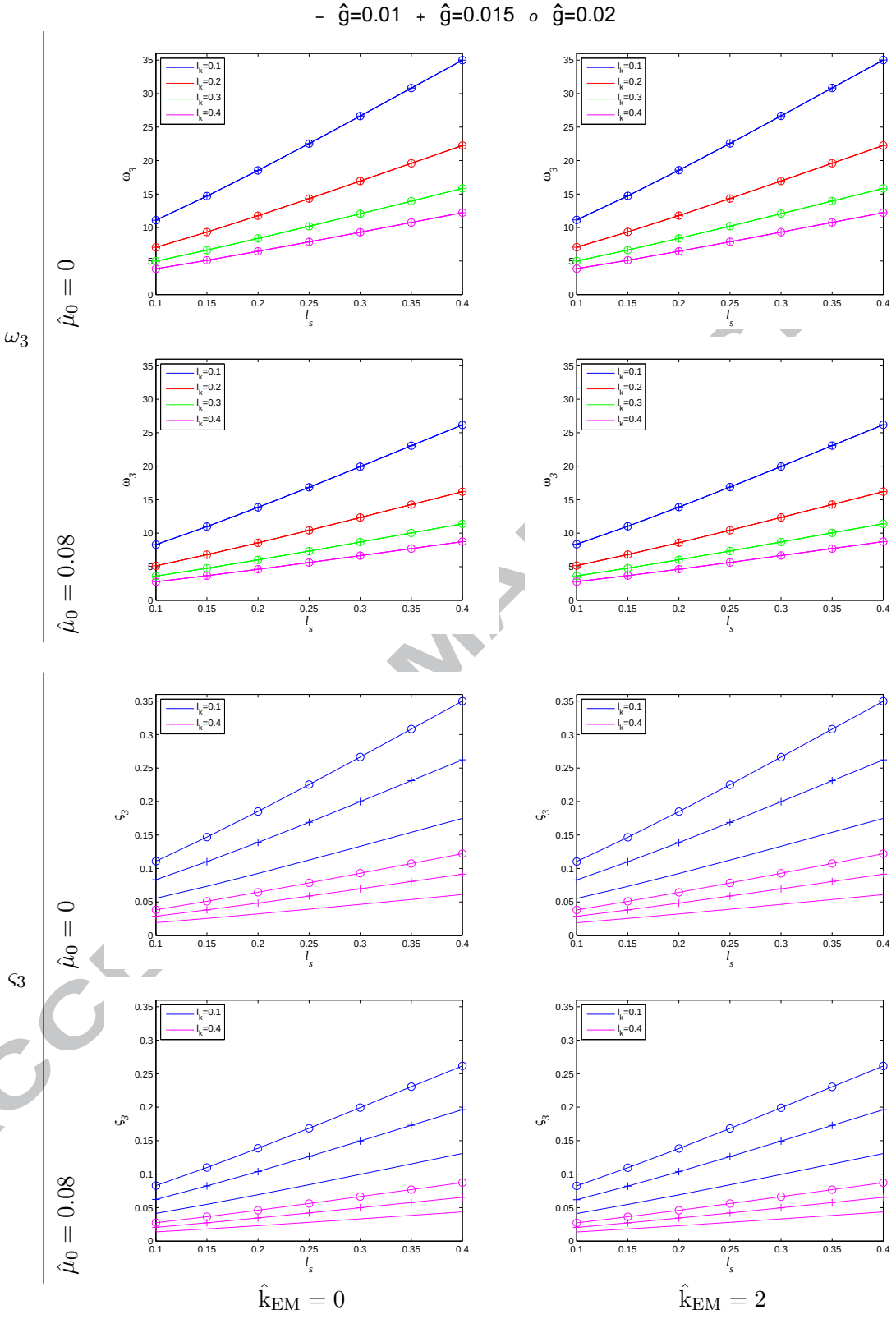


Fig. 11: Effect of length-scale parameters, stiffness of surrounding medium, and damping coefficient on the third mode frequency and damping ratio for CS-CS boundary conditions.